THE JOURNAL OF PHYSICAL CHEMISTRY C
A JOURNAL OF THE AMERICAN CHEMICAL SOCIETY

Editors' Choice
Open Access

pubs.acs.org/JPCC

Perspective

Sum-Frequency Generation Spectroscopy of Aqueous Interfaces: The Role of Depth and Its Impact on Spectral Interpretation

Published as part of The Journal of Physical Chemistry C special issue "Alec Wodtke Festschrift".

Alexander P. Fellows,* Álvaro Díaz Duque, Vasileios Balos, Louis Lehmann, Roland R. Netz, Martin Wolf, and Martin Thämer*

Cite This: J. Phys. Chem. C 2024, 128, 20733−20750

Read Online

ACCESS | Metrics & More | Article Recommendations | Supporting Information

ABSTRACT: Vibrational sum-frequency generation (SFG) has become a dominant technique in the study of molecular interfaces owing to its capabilities for molecular recognition and specificity to anisotropic structure. Nevertheless, one crucial and influential aspect of the interfacial structure, namely, its inherent three-dimensional, depth-dependent nature, cannot be obtained through conventional SFG measurements. Furthermore, not only has this depth information been so far experimentally inaccessible through SFG, the simple existence of extended anisotropic depth also complicates the analysis and interpretation of any obtained spectra. In this Perspective, we analyze the role of depth-dependent structural anisotropy in second-order vibrational spectroscopy and explore various possibilities for how the desired depth information can be experimentally attained. Using aqueous interfaces as an important and widespread example system, we highlight the prevalence of such spatially extended depth profiles, demonstrate how signals from these regions can cause significant spectral distortions, and show the entanglement between experimental parameters with the overall nonlinear response. Finally, we evaluate recently developed measurement concepts that can yield depth information, emphasizing their particular strengths, and provide an outlook for future studies employing these methodologies for the vital elucidation of depth-dependent interfacial structure.

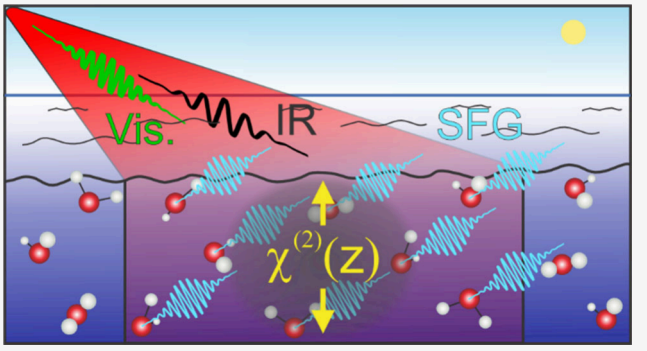

1. INTRODUCTION

Molecular interfaces are widespread across many natural and technological processes, where the unique properties of the interface strongly control their underlying function.[1−5] A central factor in determining these unique properties is the structure and dynamics of the interfacial molecules which, in contrast to the bulk, exhibit altered kinetics, orientational distributions, and intermolecular environments. Isolating the properties of this thin molecular boundary is, however, a veritable challenge requiring specialized techniques. One such technique that has been particularly elucidative is vibrational sum-frequency generation (SFG) spectroscopy. As a second-order optical process, the sign of the output SFG response (under the electric dipole approximation, EDA) is dependent on the molecular orientation, making any signals from structurally isotropic environments vanish.[6−8] For most media, this renders the technique interface-specific (in the dipolar limit), making it an excellent probe of the anisotropic interfacial structure. In addition to these symmetry selection rules, the output SFG signals also yield characteristic vibrational spectra for the molecules being probed, giving the technique molecular recognition and environment sensitivity.

While SFG investigations have led to many crucial revelations about the structure of a wide range of interfaces,[9−19] the molecular level interpretation of their spectra is nevertheless highly demanding, necessitating an exceptional understanding of the underlying theoretical concept giving rise to the signals. In this context there are two specific challenges, the first being to obtain a characteristic quantity (i.e., a material parameter) that is independent of the experimental settings and contains the desired structural information on the interface, and the second is then actually extracting the structural information from this parameter. For SFG, the material parameter governing the output signals is the second-order susceptibility, $\chi^{(2)}$.[6−8,20] Therefore, the ultimate aim of SFG measurements is to extract $\chi^{(2)}$ for the interface, more precisely its frequency dependent dipolar, vibrationally resonant part. This task is already a

Received: October 1, 2024
Revised: November 6, 2024
Accepted: November 7, 2024
Published: November 29, 2024

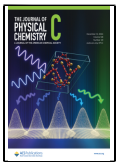

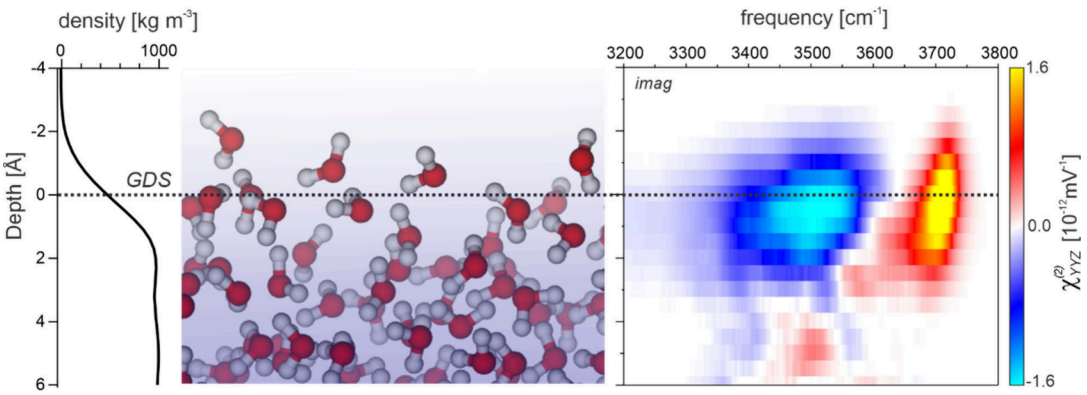

Figure 1. Snapshot of the air−water interface and the corresponding depth-dependent density and second-order susceptibility calculated from molecular dynamics simulations. The depth-dependent susceptibility highlights the regions with anisotropic structure within the interfacial layer. GDS: Gibbs dividing surface.

formidable challenge due to the common presence of nonresonant and quadrupolar signal contributions.[7,21,22] However, an additional great challenge is to remove the influence of specific experimental settings on the measured spectra, and to correctly interpret the resulting spectral information in terms of the interfacial structure. For completely homogeneous noncentrosymmetric media, this may be possible, but as soon as there is any spatial inhomogeneity, especially as a function of the distance from the interface (depth, z), $\chi^{(2)}$ will depend on the z-coordinate. In fact, in basically all applications where SFG spectroscopy is performed to investigate interfacial properties, $\chi^{(2)}$ decays to zero toward the bulk on some characteristic length-scale. As a result, the desired spectroscopic quantity that is needed to properly describe the interfacial properties is at least two-dimensional ($\chi^{(2)}(\omega, z)$). In a regular SFG experiment, however, it is not this two-dimensional quantity that is measured, but its (along z) integrated form, the effective susceptibility of the interface. Any information on the evolution of the nonlinear signal with depth is consequently lost, and with this, a large portion of the desired structural insight. Furthermore, this integration can also lead to important distortions of the vibrational line-shapes which obstruct an unambiguous interpretation of the obtained spectra. Finally, the integration in z leads to an intrinsic convolution between the nonlinear responses and experimental parameters (such as angle(s) of incidence) that cannot be disentangled without precise depth information. In order to obtain a fully unbiased view on interfacial molecular structures it is therefore clear that suitable experiments should additionally include depth information.

In this Perspective, we directly discuss the impact of the depth dependency of $\chi^{(2)}(\omega, z)$ in SFG investigations, with a specific focus on one particularly prevalent class of interfaces, namely those involving water. It is divided into four main sections. In section 2, the role of depth is examined by considering its connection to the accessible quantity in SFG measurements, with examples discussed for the pure air−water interface as well as those with a net surface charge. In doing so, we also explicitly demonstrate the entangled nature of the material properties with experimental parameters, showing how signal contributions from nonzero depth generally lead to their inseparability. Thereafter, in section 3, we critically explore how structural information can be extracted from measured SFG spectra, focusing particularly on both the nonresonant contribution and quadrupolar mechanisms, showing how they are linked to depth and can alter the structural interpretations of any obtained spectra. With these important discussion points in hand, we review in section 4 the latest developments in SFG spectroscopy in terms of overcoming some of these complications and gaining access to depth information. Finally, in section 5, we then discuss the potential of these methods in the perspective of the future directions for more advanced structural interpretations at aqueous interfaces.

2. THE IMPORTANCE OF DEPTH IN SFG MEASUREMENTS

The structural anisotropy at interfaces and its evolution with depth is a prominent and defining parameter controlling many properties. Due to its selection rules, SFG primarily probes this anisotropy, so the depth-dependent $\chi^{(2)}(z)$ that governs the output SFG signals is directly representative of the depth-dependent anisotropy at the interface. In this section, we present the structural insight that can be gained by accessing $\chi^{(2)}(z)$, and analyze the relation between the measured signal and this quantity, as well as how depth is intrinsically intertwined in their relation.

2.1. The 2D "Picture" of the Interface. State-of-the-art molecular dynamics (MD) simulations can generally yield the complete spatially resolved (2D) susceptibility ($\chi^{(2)}(z)$), and thus give a "full" picture of the interfacial region.[23−25] An example of this is shown in Figure 1 for the air−water interface, including a snapshot of an *ab initio*-parametrized MD simulation of the structural transition between the two phases and the calculated depth and frequency-resolved 2D second-order susceptibility, shown in the O−H stretching region.

This 2D picture of the interfacial structure clearly shows the same spectral features as observed from previous phase-resolved SFG measurements of the air−water interface,[24,26−30] with a sharp positive (yellow/red) resonance at ∼3700 cm^{-1} arising from non-H-bonded ("free") OH groups pointing "up" toward the air phase and a broader negative (cyan/blue) resonance at ∼3400−3600 cm^{-1} from H-bonded OH groups pointing "down" toward the bulk water phase. Beyond this, however, far more insight can be obtained from this spatially resolved picture. For example, the entire SFG signal arises from a region of ∼6 Å, corresponding to 2−3 molecular layers, showing that the entire structural anisotropy is restricted to this region. Furthermore, it is clear that both of the aforementioned moieties exist through this entire region since both the positive and negative signals appear from the same depths. This shows, for

https://doi.org/10.1021/acs.jpcc.4c06650
J. Phys. Chem. C 2024, 128, 20733−20750

example, that the picture of a sharp transition between the gas and condensed phases with the topmost condensed layer containing all of the "free" OH and the molecules beneath solely contributing strongly H-bonded signals is clearly inaccurate.[30−33] On closer inspection, there is some slight indication of the "free" OH signal starting from closer to the air-phase than the H-bonded signal, aligning with expectation, but also that both contributions appear to somewhat red-shift on increasing depth, indicating a gradient in H-bonding strength when approaching the bulk. This observation is in line with the idea of the interface having a "healing depth" over which the loss of H-bonding induced by the interface is recovered.[24,31] Overall, Figure 1 clearly showcases the complementary information obtained by comparing the simulation snapshot and its associated temporally averaged density profile with the calculated second-order susceptibility $\chi^{(2)}(z)$. The former clearly embodies the molecular density, its inhomogeneities, and specific local structural motifs. However, the anisotropy in molecular orientation and interconnectivity only becomes apparent upon inspection of the $\chi^{(2)}(z)$ image.

2.2. The Experimentally Accessible Quantity in SFG. Evidently, having access to the depth dependency of $\chi^{(2)}(z)$ would provide a highly detailed structural view of the interface. Regular SFG measurements, however, do not yield this two-dimensional quantity, but rather a single spectrum of the output SFG field that often has some characteristic line-shape from which structural information can be inferred. As it is not the second-order susceptibility that is measured, it is thus important to know how the obtained SFG signals precisely relate to the intrinsic properties of the medium, i.e., what exactly is the measured quantity in an SFG experiment?

Generally, the output SFG field (under the EDA) is produced by the induced second-order polarization oscillating at the SFG frequency, $p^{(2)}(\omega_3 = \omega_2 + \omega_1)$, which is generated by the coupling of the two incident fields, E_1 and E_2, as in eq 1,

$$p^{(2)}(\omega_3 = \omega_2 + \omega_1) = \epsilon_0 \chi^{(2)}(\omega_3, \omega_2, \omega_1) E_2 E_1 \tag{1}$$

where ϵ_0 is the vacuum permittivity.[6−8,20,34,35] Importantly, however, the detectable quantity rather arises from the sum of all individual second-order polarization in the medium, hence represented by a 3D spatial integral, as in eq 2.

$$P^{(2)}_{\text{eff}} = \int_V p^{(2)} \, \mathrm{d}V \tag{2}$$

Given that the vast majority of substrates, including aqueous systems, possess in-plane homogeneity, contributions from the same depth (distance from the interface) are only modulated by the lateral field distribution (e.g., spatial beam profile and spot size). Thus, the lateral integration in eq 2 can be typically reduced to a beam-dependent amplitude prefactor. For contributions arising from different depths, however, not only are the local structures potentially different, leading to differing induced local second-order polarizations, but the input and output beams also have an increased path length. This increased beam propagation results in a depth-dependent phase shift (propagation phase) that is linked to the z-component of the wave-vector mismatch (reciprocal of the coherence length), Δk_z, which must be incorporated into the spatial integral.[24,36−38] Overall, therefore, the detectable output field is actually governed by an effective second-order susceptibility, $\chi^{(2)}_{\text{eff}}$, that is given by eq 3.

$$\chi^{(2)}_{\text{eff}} = \int_0^\infty f_3(z) f_2(z) f_1(z) \chi^{(2)}(z) \, \mathrm{e}^{i\Delta k_z z} \, \mathrm{d}z \tag{3}$$

This definition also includes the local field correction factors, $f(z)$, to account for the dielectric inhomogeneity which must also be present at the boundary between the two bulk phases.[7] As the integral in eq 3 cannot be generally solved, the accessible quantity in SFG measurements is restricted to this integrated quantity. In consequence, the entire depth information is inaccessible through regular SFG measurements.

2.3. Obtaining Absolute Units. While the effective susceptibility given in eq 3 represents the accessible quantity in SFG measurements, it is still not the measured quantity, as this also includes the strength of the incident fields and an instrument-dependent prefactor. In order to extract the pure $\chi^{(2)}_{\text{eff}}$ from a measurement, therefore, the measured signals must be referenced. This is usually achieved by comparing the measured signal to the analogous output from a bulk nonlinear crystal.[39] In doing so, therefore, the obtained spectra can also be converted into absolute units by using the known value for the second-order susceptibility of the reference, e.g., for z-cut quartz, the aaa tensor component of the second-order susceptibility (using the coordinates defined by its crystal symmetry) is widely accepted to be 6×10^{-13} m V^{-1}.[8] As the *effective* susceptibilities for both sample and reference are depth-integrated quantities, and therefore formally not true second-order susceptibilities, it is important to notice that they also possess different units: m^2 V^{-1} instead of m V^{-1} as for the regular second-order susceptibility. Therefore, for proper referencing and obtaining absolute units for the sample response, the known reference susceptibility must also be combined with experimental parameters (e.g., angle(s) of incidence) and integrated, just as in eq 3, effectively leading to a coherence length-modulated amplitude.

The two responses, sample (S^{s}) and reference (S^{ref}), can be written as in eqs 4 and 5, respectively, with the indices i, j, k representing the specific spatial components of the fields and susceptibility tensor, and L_n being the Fresnel factors for the input and output beams which account for the change in field amplitudes between the incident and sample medium.

$$S^{\text{s}} \propto I_{\text{s}}(\theta) L^{\text{s}}_i(\omega_3) L^{\text{s}}_j(\omega_2) L^{\text{s}}_k(\omega_1) \times \int_0^\infty f^{\text{s}}_i(\omega_3, z) \, f^{\text{s}}_j(\omega_2, z) f^{\text{s}}_k(\omega_1, z) \chi^{(2),\text{s}}_{ijk}(z) \, \mathrm{e}^{i\Delta k_z z} \, \mathrm{d}z \, E(\omega_2) E(\omega_1) \tag{4}$$

$$S^{\text{ref}} \propto I_{\text{ref}}(\theta) L^{\text{ref}}_i(\omega_3) L^{\text{ref}}_j(\omega_2) L^{\text{ref}}_k(\omega_1) \times \int_0^\infty f^{\text{ref}}_i(\omega_3, z) \, f^{\text{ref}}_j(\omega_2, z) f^{\text{ref}}_k(\omega_1, z) \chi^{(2),\text{ref}}_{ijk}(z) \, \mathrm{e}^{i\Delta k_z z} \, \mathrm{d}z \, E(\omega_2) E(\omega_1) \tag{5}$$

Here, these signals are given neglecting the instrument-dependent proportionality constant (being the same for both sample and reference), but include a prefactor, $I(\theta)$, to account for the dependency of the output on the incident angle, with its functional form also depending on the specific tensor element being probed (i.e., the spatial components of the incident and output fields). As an example, using quartz as a reference in the commonly used SSP polarization combination, eqs 4 and 5 can be rewritten as in eqs 6 and 7. Note, as the susceptibility for the reference is constant, the integral can be directly solved.

https://doi.org/10.1021/acs.jpcc.4c06650
J. Phys. Chem. C 2024, 128, 20733−20750

$$S^{s} \propto \sin\theta L_y^{s}(\omega_3)L_y^{s}(\omega_2)L_z^{s}(\omega_1) \times \int_0^{\infty} f_y^{s}(\omega_3, z) f_y^{s}(\omega_2, z) f_z^{s}(\omega_1, z)\chi_{yyz}^{(2),s}(z)\, e^{i\Delta k_z z}\, dz\, E(\omega_2)E(\omega_1) \quad (6)$$

$$S^{Q} \propto \cos\theta L_y^{Q}(\omega_3)L_y^{Q}(\omega_2)L_x^{Q}(\omega_1) \times \int_0^{\infty} f_y^{Q}(\omega_3, z) f_y^{Q}(\omega_2, z) f_x^{Q}(\omega_1, z)\chi_{yyx}^{(2),Q}(z)\, e^{i\Delta k_z z}\, dz\, E(\omega_2)E(\omega_1) = L_y^{Q}(\omega_3)L_y^{Q}(\omega_2)L_x^{Q}(\omega_1)\frac{i}{\Delta k_z}\chi_{yyx}^{(2),Q}E(\omega_2)E(\omega_1) \quad (7)$$

Here, the SSP polarization combination probes both the YYX and YYZ tensor components, with the former vanishing in the case of in-plane isotropy.[6−8,20] Therefore, for typical sample interfaces such as aqueous systems, the YYZ component is the only contribution. In contrast, z-cut quartz yields the YYX contribution in SSP.[40] Division of the two responses then yields the expression in eq 8 that has removed any field dependency and thus provided a known amplitude and phase reference.

$$\frac{S^{s}}{S^{Q}} = \tan\theta \frac{L_y^{s}(\omega_3)L_y^{s}(\omega_2)L_z^{s}(\omega_1)}{L_y^{Q}(\omega_3)L_y^{Q}(\omega_2)L_x^{Q}(\omega_1)} \frac{\Delta k_z}{i\chi_{yyx}^{(2),Q}} \int_0^{\infty} f_y^{s}(\omega_3, z) f_y^{s}(\omega_2, z) f_z^{s}(\omega_1, z)\chi_{yyz}^{(2),s}(z)\, e^{i\Delta k_z z}\, dz \quad (8)$$

Rearrangement of eq 8 then yields the accessible quantity of interest for the sample ($\chi_{eff}^{(2)}$), as in eq 9.

$$\chi_{eff}^{(2)} = \int_0^{\infty} f_y^{s}(\omega_3, z) f_y^{s}(\omega_2, z) f_z^{s}(\omega_1, z)\chi_{yyz}^{(2),s}(z)\, e^{i\Delta k_z z}\, dz = \cot\theta \frac{L_y^{Q}(\omega_3)L_y^{Q}(\omega_2)L_x^{Q}(\omega_1)}{L_y^{s}(\omega_3)L_y^{s}(\omega_2)L_z^{s}(\omega_1)} \frac{i\chi_{yyx}^{(2),Q}}{\Delta k_z} \frac{S^{s}}{S^{Q}} \quad (9)$$

This expression can then be used to yield absolute units by using known values for the susceptibility of z-cut quartz (taken to be 6×10^{-13} m V^{-1}, as mentioned above), the wavevectors of the incident beams, and calculated Fresnel factors (e.g., using the two- or three-layer model[7]). Importantly, eq 9 highlights that referencing by simple dividing the sample spectrum by the quartz response does not correctly scale the amplitudes. This is clear, for example, as the amplitude scaling of the quartz response is dependent on the coherence length and thus is highly sensitive to the experimental settings and the specific probing frequencies. Therefore, by simply dividing by the quartz response, this dependency on input frequencies and experimental settings enters into the obtained sample spectrum. Instead, by implementing the referencing shown in eq 9, these effects are accounted for, along with the impact of the incidence angle and Fresnel factors.

The above discussion shows that proper referencing is not a straightforward task, requiring not just a simple division but also the incorporation of the beam geometry and frequency-dependent coherence length and Fresnel factors. Nevertheless, reporting spectra in absolute units (m^2V^{-1}) has crucial benefits as it enables better comparisons between the results from different experimental setups, as well as testing the accuracy of simulations. In general, the absolute amplitude of the susceptibility is determined by three factors. First, there is obviously the intrinsic size of the molecular hyperpolarizability, second, there is the density of noncanceling chromophores per molecular layer, which reports on the amount of orientational order, and finally there is the number of contributing molecular layers, i.e. the anisotropic depth. Therefore, being able to compare the absolute amplitudes of SFG signals from different systems gives some insight into these structural parameters. In principle, different samples can be categorized as one of three distinct cases: (i) those with only a single (or very thin) contributing layer, (ii) those with effectively infinite contributions in depth (e.g., for non-centrosymmetric crystals such as quartz), and (iii) anything in between.

An example of comparing two systems in the category (i) is given in Figure 2 which shows the imaginary parts of the SFG spectra recorded in the O−D stretching region for the air-D_2O interface and the C−H stretching region for a self-assembled monolayer of octadecyltrichlorosilane (OTS) formed on fused silica. These spectra are first shown alongside one another in arbitrary units (black traces) in a similar fashion to what is commonly presented in the literature.[41−47] Only when compared in absolute units however (as shown underneath in red), does it become clear that the OTS CH_3 resonances from the terminal methyl group that dominate the spectrum are substantially stronger than the signals from the air−water interface. This is remarkable given that the O−D stretch response of water has a significantly larger molecular hyperpolarizability than aliphatic C−H stretches, similar interfacial density, and even has 2−3 contributing layers rather than just 1, as for OTS.[24] The weak signals from water thus show that the interfacial structure must contain either a significant amount of canceling out-of-plane contributions, suggesting a broad orientational distribution, or a substantial in-plane structure (which also cancel and yield no net SFG signal). It is therefore clear that there cannot be a significant preferential out-of-plane orientation of water molecules at the interface. These

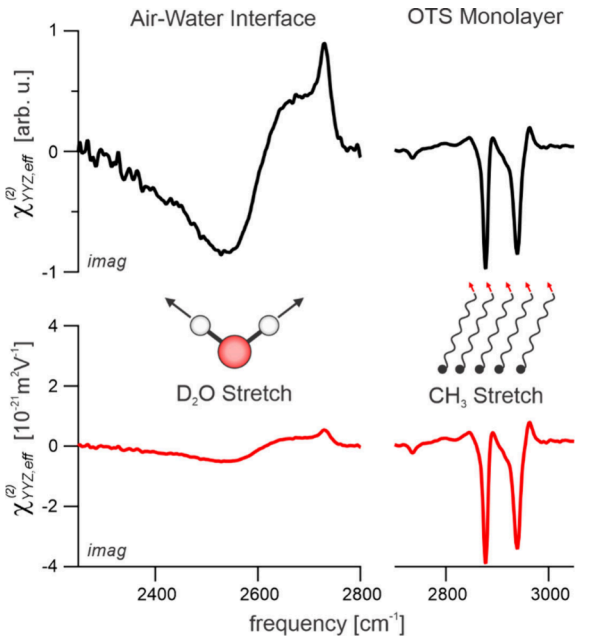

Figure 2. Imaginary parts of the heterodyned SFG spectra recorded in the SSP polarization combination for the air-H_2O interface in the H−O−H bending region, air−D_2O interface in the O−D stretching region, and OTS self-assembled monolayer on fused silica in the C−H stretching region. Reprinted in part with permission from ref 24. Copyright 2024 American Chemical Society.

https://doi.org/10.1021/acs.jpcc.4c06650
J. Phys. Chem. C 2024, 128, 20733−20750

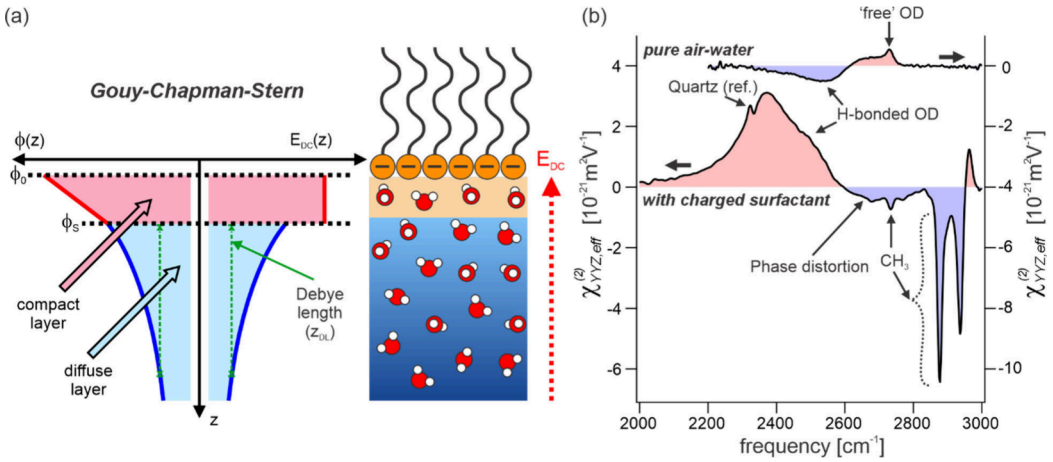

Figure 3. SFG from charged interfaces showing (a) a schematic of the Gouy-Chapman-Stern model describing the electrostatics of the interfacial region, with the depth evolution of the electric field and potential as well as the two-layer regime, and (b) imaginary parts of the heterodyned SFG spectra of the pure air−water interface (right axis) and that covered with a negatively charged surfactant monolayer (dihexadecylphosphate, DHP, left axis), thus with no added subphase electrolyte, both recorded in the SSP polarization combination. The sharp positive contribution at ∼2320 cm^{-1} is not a feature of the sample, but arises from the spectral referencing to quartz. Reprinted in part with permission from ref 24. Copyright 2024 American Chemical Society.

observations align with expectation and other findings from simulations, which suggest that a majority of the water dipoles at the interface lie in-plane, and the residual out-of-plane populations are almost equally distributed between "pointing up" and "pointing down".[33] However, such insight into the structural properties of the interface only becomes possible from an analysis of the SFG signals reported in absolute values.

While this analysis of the SFG amplitudes from systems in category (i) can be used to obtain important structural information, this can, however, not be generalized to include other systems in category (iii). In such cases, the amplitudes are modulated both by the orientational distribution and the thickness of the anisotropic structure (number of contributing layers). Therefore, without depth information, insight into the orientational distributions cannot be extracted.

2.4. Charged Interfaces. Prominent examples with $\chi^{(2)}(z)$ extending up to 100s of nanometers in depth (i.e., category (iii) above) are charged aqueous interfaces, where the electric field induces far-reaching structural anisotropy. These are found in numerous relevant systems ranging from physiological membranes and oceanic surfaces, to electrochemical devices, thus being of enormous scientific and technological interest.[48] As such, many SFG investigations have been performed on charged interfaces to elucidate their structural and dynamical properties.[14,48−53] As the role of depth in the SFG spectra from such systems becomes immensely influential, however, interpretation of the obtained data remains challenging.

The presence of such excess surface charge generates a static electric field which can penetrate into the bulk water and act on any electric charges or dipoles, resulting in altered ion distributions and, importantly, the alignment of strongly dipolar water molecules. This field-induced orientational order within the otherwise isotropic water environment can thus give rise to SFG signals originating several 100s of nm away from the interface.[38]

The theoretical description of the response from charged interfaces can be found in many places in the literature.[38,51,54−56] However, it is important to note that in many cases, the presented derivations are shown with a final equation that neglects aspects about the depth-dependent electrostatics in such systems and their connection to the SFG responses.[38,51,55,56] It is therefore important to present the derivation and its associated assumptions in full detail so as to avoid any future misconceptions.

If we include the field-induced response, the effective susceptibility becomes as in eq 10, with $E_{DC}(z)$ being the static (DC) field from the interface which is combined with a third-order susceptibility, $\chi^{(3)}$, to generate SFG photons.[38,49,55] This description comes from including the first term in the Taylor expansion with the DC field, thus in the limit of the response of water to the field being linear.

$$\chi^{(2)}_{\text{eff}} = L_3L_2L_1 \int_0^\infty f_3(z)f_2(z)f_1(z)(\chi^{(2)}(z) + \chi^{(3)}(z)\cdot E_{DC}(z))\, e^{i\Delta k_z z}\, dz \tag{10}$$

The resulting integral can clearly be split into two components, with the first arising from the direct solvation (chemistry driven) $\chi^{(2)}$ contribution that behaves the same as in the earlier discussion and generally will only be relevant over a few molecular layers, and the second being the field-dependent $\chi^{(3)}$ contribution which follows the depth of the static electric field, thus potentially representing 1000s of molecular layers. It is this latter contribution, therefore, that makes depth a crucial parameter in SFG measurements from such systems.

In order to evaluate the field-induced contribution, it is important to note that the static field is nothing other than the negative gradient of the electric potential, ϕ, allowing eq 10 to be rewritten as in eq 11.

$$\chi^{(2)}_{\text{eff}} = L_3L_2L_1 \int_0^\infty f_3(z)f_2(z)f_1(z)\left(\chi^{(2)}(z) - \chi^{(3)}(z)\cdot \frac{d\phi(z)}{dz}\right) e^{i\Delta k_z z}\, dz \tag{11}$$

Clearly, however, to perform the integration, not only does the depth-dependency of both susceptibilities need to be known, but also that of the electric potential. For this, it is common to resort to electrostatic models of the interface such as the Gouy-Chapman-Stern (GCS) model, a schematic of which is

https://doi.org/10.1021/acs.jpcc.4c06650
J. Phys. Chem. C 2024, 128, 20733−20750

presented in Figure 3a.[48,57−62] This shows two distinct electrostatic regimes, the compact layer (CL, often also referred to as the Stern layer, SL, or bonded interfacial layer, BIL[54,56,63,64]) in the immediate vicinity of the surface charges which accounts for direct solvation at the interface, and a second regime beneath, the diffuse layer (DL), which describes the screening of the residual electric field due to dissolved ions in an otherwise bulk-like environment, with the characteristic Debye length, z_{DL}. Within the GCS model description, the CL acts as a pseudocapacitor and thus presents a linearly changing electric potential from the surface (ϕ_0) to the Stern layer (ϕ_S, sometimes also referred to as the outer Helmholtz potential[65,66]), after which it decays exponentially in the DL due to screening.

In the GCS model, however, the molecular nature of water is neglected, with its role being treated as a homogeneous dielectric medium.[48] The impact the molecular water interactions have on the electrostatic potential in the system is a complex problem and it is thus hard to evaluate the accuracy of this approximation. Nevertheless, the GCS model likely represents a reasonable mean field approach for describing the water response as any inherent anisotropy induced by the presence of the interface and any direct solvation to the charged headgroup or their counterions should be contained within the CL, being represented as by $\chi^{(2)}$. On the other hand, both the CL and DL can generate field-induced responses, which can be distinguished not only because they likely have different electrostatic regimes, but also different molecular structures (and thus potentially different susceptibilities). The overall effective susceptibility can therefore be written as in eq 12, including distinct $\chi^{(3)}$ tensors for the two layers.

$$\chi^{(2)}_{\text{eff}} = L_3L_2L_1 \int_0^{\infty} f_3(z)f_2(z)f_1(z)\left(\chi^{(2)}_{\text{CL}}(z) - (\chi^{(3)}_{\text{CL}}(z) + \chi^{(3)}_{\text{DL}}(z))\cdot\frac{\mathrm{d}\phi(z)}{\mathrm{d}z}\right) \mathrm{e}^{i\Delta k_z z}\,\mathrm{d}z \tag{12}$$

The integral in eq 12 can be split across the two distinct layers, separated at the Stern layer boundary, z_S, resulting in eq 13 where two simplifying assumptions have been made. First, as the DL structure can be assumed to be isotropic in the absence of the field, any depth dependence to $\chi^{(3)}_{\text{DL}}$ is neglected. Second, as the CL is typically much thinner than the coherence length, any propagation phase is very small and can thus be neglected in such a case (see Supporting Information).

$$\chi^{(2)}_{\text{eff}} = \int_0^{z_S} \chi^{(2)}_{\text{CL}}(z) - \chi^{(3)}_{\text{CL}}(z)\cdot\frac{\mathrm{d}\phi(z)}{\mathrm{d}z}\,\mathrm{d}z - \chi^{(3)}_{\text{DL}} \cdot\int_{z_S}^{\infty} \frac{\mathrm{d}\phi(z)}{\mathrm{d}z}\,\mathrm{e}^{i\Delta k_z z}\,\mathrm{d}z \tag{13}$$

While performing the integration over the CL contributions requires knowledge of the depth-dependency of the CL water structure (i.e., both susceptibilities) and thus cannot be generally performed, the integration over the DL can be evaluated just with knowledge of the depth-dependent potential. With the potential being described by eq 14 under the GCS model, integration by parts then yields eq 15 for the effective susceptibility, with the overall integrated CL contribution being written as an effective susceptibility from this region, $\chi^{(2)}_{\text{CL,eff}}$.

$$\phi(z) = \begin{cases} \phi_0 - \dfrac{(\phi_0 - \phi_S)}{z_S} z & 0 < z \le z_S \\ \phi_S\,\mathrm{e}^{-(z-z_S)/z_{DL}} & z \ge z_S \end{cases} \tag{14}$$

$$\begin{aligned} \chi^{(2)}_{\text{eff}} &= \chi^{(2)}_{\text{CL,eff}} - \chi^{(3)}_{\text{DL}}\cdot\left([\phi(z)\,\mathrm{e}^{i\Delta k_z z}]_{z_S}^{\infty} - i\Delta k_z \int_{z_S}^{\infty} \phi(z)\,\mathrm{e}^{i\Delta k_z z}\mathrm{d}z\right) \\ &= \chi^{(2)}_{\text{CL,eff}} - \chi^{(3)}_{\text{DL}}\cdot\left(-\phi_S\,\mathrm{e}^{i\Delta k_z z_s} - i\Delta k_z \phi_S \mathrm{e}^{i\Delta k_z z_s}\int_0^{\infty} \mathrm{e}^{(-1/z_{DL}+i\Delta k_z)z}\,\mathrm{d}z\right) \\ &= \chi^{(2)}_{\text{CL,eff}} + \phi_S\,\chi^{(3)}_{\text{DL}}\,\mathrm{e}^{i\Delta k_z z_S}\cdot\left(1 + \frac{i\Delta k_z}{\frac{1}{z_{DL}} - i\Delta k_z}\right) \\ &\approx \chi^{(2)}_{\text{CL,eff}} + \phi_S\,\chi^{(3)}_{\text{DL}}\cdot\left(\frac{1}{1 - i\Delta k_z z_{DL}}\right) \\ &= \chi^{(2)}_{\text{CL,eff}} + \frac{1}{2}\phi_S\,\chi^{(3)}_{\text{DL}}\cdot(1 + \mathrm{e}^{2i\mathrm{atan}(\Delta k_z z_{DL})}) \end{aligned} \tag{15}$$

In the fourth line of eq 15, the propagation phase associated with the CL thickness, z_S, is once again neglected as it will generally make little impact due to the CL thickness being small compared to the coherence length (see Supporting Information for details). Importantly, eq 15 shows that the DL contribution contains potentially large phase-shifts depending on the Debye length, and is modulated by the Stern potential, ϕ_S, and not the surface potential, ϕ_0, as is frequently stated in various publications.[14,67−71] This distinction, having been also noted previously in passing,[29,54,66] naturally arises from the fact that the DL field does not start directly at the charged surface, but **below** the CL at the boundary to the DL. While this inaccuracy may seem trivial, the large potential drop across the CL makes this difference in fact substantial. Therefore, using the correct expression is crucial for an accurate electrochemical description of the interface and any thermodynamic quantity extracted from such measurements, for example surface charge density or local pK_a.[50]

Eq. 15 highlights the role that depth contributions play in the SFG spectra from charged interfaces. Specifically, it shows that the presence of the static field adds a second, potentially significant, contribution to the overall response arising from larger depths which could have a substantially different spectral line-shape for two reasons. First, the DL contribution arises from water in a different molecular environment compared to the CL, thus could show frequency shifts and bandwidth changes to the resonant features. Second, as the DL contribution is phase-shifted (originating from the propagation phase) by a potentially significant amount dependent on the Debye screening length (and thus the salinity of the system), the spectral line-shape will be distorted.

An example of these effects is given in Figure 3b which shows the SFG spectra for the pure air-D_2O interface (just as in Figure 2) as well as that covered with a monolayer of a negatively charged surfactant (dihexadecylphosphate, DHP). On first comparison, the two spectra appear substantially different. Unlike the pure air−water interface, the surfactant-covered interface shows strong, sharp resonances between 2800 and 3000 cm^{-1} which predominantly arise from the terminal CH_3 groups of the well-packed surfactant monolayer.[20] Beyond this, however, the water response (in the lower frequency range, <2700 cm^{-1}) also appears notably different. Specifically, the OD resonances appear highly red-shifted, falling at ∼2400 cm^{-1} compared to ∼2550 cm^{-1} for pure air−water, significantly larger in amplitude, and entirely positive (unlike pure air−water which

https://doi.org/10.1021/acs.jpcc.4c06650
J. Phys. Chem. C 2024, 128, 20733−20750

shows significant positive and negative resonances). These observations align well with expectations at the charged interface as the solvation of the charged surfactant head-groups and DL contribution will present greater overall H-bonding compared to the hydrophobic air interface, lowering the overall resonant frequency.[72−74] Furthermore, the static field will cause significant orientational alignment of water, thus boosting the amplitude, and the alignment with the field from the negatively charged interface will be such that the molecular dipoles are pointing "up", yielding only positive resonances. Finally, and importantly, while the pure air−water spectrum will show no noticeable phase distortion as it arises from an ultrathin interfacial layer, the spectrum from the charged interface clearly shows a broad negative feature above the main (positive) resonance, between 2600 and 2800 cm^{-1}. This dip-like feature is a clear manifestation of a depth-related phase distortion, with some of the dispersive (real) line-shape entering into the imaginary part. Overall, this demonstrates that the large Debye length associated with having low salinity conditions in this sample leads to significant effects on the line-shape of the overall response.

2.5. Entanglement with Experimental Parameters. From the above discussion on a specific class of sample system where depth is highly relevant, we now turn to a fundamental consequence of the integrated nature of the effective susceptibility. As shown in eq 3, $\chi^{(2)}_{eff}$ is a function of the coherence length, which is a parameter that depends on the experimental settings such as the specific beam geometry and input frequencies of the probing fields. As such, two measurements with varying coherence lengths can yield very different spectra. This dependency of $\chi^{(2)}_{eff}$ on Δk_z cannot simply be removed since the terms containing the coherence length are functions of the integration variable so they cannot be moved outside the integral and therefore their values directly influence the line-shape of the obtained spectra. Hence, the depth-dependent structure and the experimental settings are entangled in the observed response. However, the impact of this entanglement is highly variable.

In the case that the interfacial signals originate entirely from a negligibly thick layer (which could be approximated by a delta function, category (i) above), there is no significant propagation phase to be considered and the sensitivity to experimental parameters would almost completely vanish on the assumption of minimal dispersion for the nonresonant fields. In such cases, the $\chi^{(2)}_{eff}$ spectra (when considering only a single contributing tensor component) obtained from measurements with varying experimental settings should be identical, with examples being OTS on fused silica or even the resonant O−D stretching response of the air−water interface where only ∼2−3 molecular layers form the anisotropic structure.[75] The added propagation phase for such a thickness is negligible for typical values of the coherence length (e.g., for $z < 1$ nm and $\frac{1}{\Delta k_z} \sim 50$ nm, the added propagation phase is contained with ∼1°). Therefore, the resulting SFG spectra here show minute phase distortions and the signals from each layer are essentially purely additive.

However, the moment where nanoscale depth contributions are present (e.g., for water at charged interfaces), the spectra from measurements employing different experimental settings will significantly deviate due to the modulation of the signals from different depths by propagation phase-shifts and local field corrections. In this case, it is impossible to remove the impact of the experimental parameters and report an unbiased single spectrum that could easily be compared to other measurements with different experimental settings (frequencies, geometry, etc.). The only characteristic, unbiased "spectrum" would be the experimentally inaccessible full two-dimensional representation, $\chi^{(2)}(z)$, which can typically only be obtained from simulations. As shown in section 4, however, advanced methods can recover some of this information by modulating contributions from different depths.

3. COMPLICATIONS FOR STRUCTURAL INTERPRETATIONS AND MOLECULAR RECOGNITION

In the previous section, we emphasized the difference between the idealized measured quantity, the 2D second-order susceptibility, and the true measured quantity in experimental SFG investigations, namely the spatially integrated signal. In doing so, we highlighted the critical role that depth plays in the response, entangling the material properties with experimental parameters and leading to potentially significant line-shape distortions. In this section, we will now turn to an examination of the challenges for identifying specific molecular motifs and obtaining structural information from this measured quantity. Specifically, we discuss the impact of possible line-shape distortions that can originate from the depth-integrated nature of the effective second-order susceptibility (as mentioned above), but also from the interference from multiple sources, including the vibrationally resonant response with other nonlinear signal contributions. These cases are each individually addressed in the following and their impact is demonstrated using specific examples.

3.1. Depth Related Line-Shape Distortions. The interpretation of spectral features within a measured SFG spectrum can easily be misled by the presence of phase distortions. As phase-shifts lead to mixing between real (dispersive) and imaginary parts (absorptive) of the vibrational line-shapes, single resonance peaks can appear as doublets (dip-peak features) in a measured spectrum. As an example, we refer to the spectrum of charged water interfaces in Figure 3b. The spectrum could easily be evaluated without considering this effect, concluding that the negative feature between 2600 and 2800 cm^{-1} arises from a weakly H-bonded water environment with pointing "down" molecular dipoles. This conclusion, however, contradicts expectations given that the negatively charged interface leads to a strong preference for pointing "up" molecules, and pointing "down" molecules would not be expected to have such weak H-bonding.[69,76] In reality, this negative feature simply originates from the dispersive (real) part of the intrinsic sample response that enters the measured imaginary spectrum through depth-induced phase-shifts. This example clearly demonstrates that a correct interpretation of the observed spectral features requires at least some knowledge on the length-scale on which the nonlinear signal contributions decay as a function of depth.

3.2. Interference between Multiple Contributions. Many sample systems of interest contain multiple SFG contributions that can have very different spatial origins, e.g. CL and DL from charged aqueous interfaces, as in the example discussed above. The presence of such multiple contributions can also lead to major challenges in the data analysis. Within the example above (charged aqueous interfaces), it is important to point out that even with information on the depth evolution in hand, it is not possible to simply phase-correct the obtained overall SFG spectra and evaluate the unperturbed spectrum. As

https://doi.org/10.1021/acs.jpcc.4c06650
J. Phys. Chem. C 2024, 128, 20733−20750

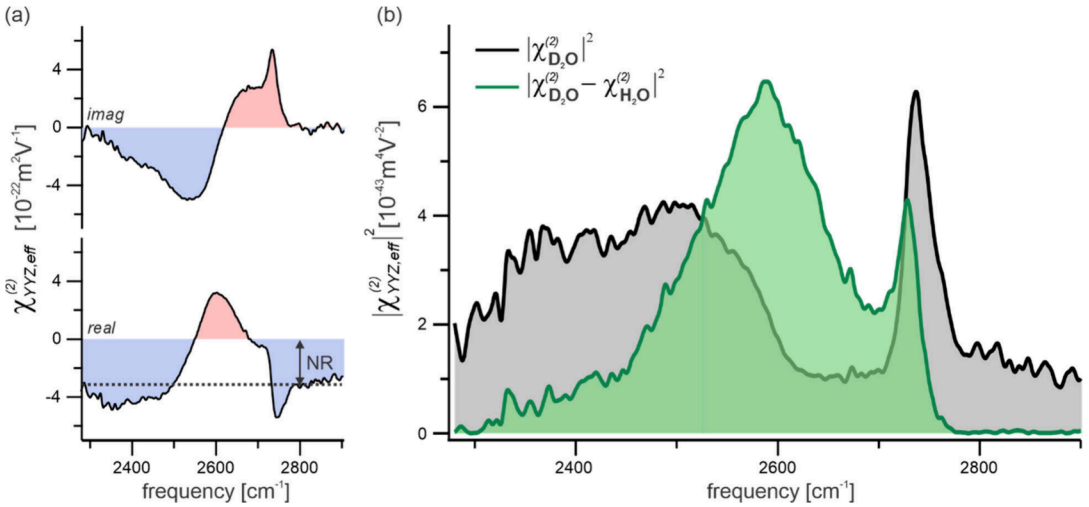

Figure 4. SFG spectra of the air−D_2O interface recorded in the SSP polarization combination showing (a) phase-resolved response split into real and imaginary parts, highlighting the significant nonresonant contribution (NR), and (b) intensity spectrum for the overall response (resonant + nonresonant) and the resonant-only response, having subtracted the H_2O NR spectrum. Reprinted in part with permission from ref 24. Copyright 2024 American Chemical Society.

shown in eq 15, the overall SFG response from such an interface is composed of two contributions, one from the CL and a second contribution from the DL. As only the second contribution contains significant phase-shifts, the only way to remove the effect of depth induced phase distortions is to first correctly decompose the overall spectrum into CL and DL contributions and subsequently only phase-correct the DL spectrum. Such a decomposition clearly cannot be done based on a single SFG measurement.

In their recent work, however, Gibbs and co-workers showed that, by combining phase-resolved SFG spectra with heterodyned, off-resonant second harmonic generation (SHG) and streaming current measurements, the two components (CL and DL) can be isolated.[65,77] Furthermore, by using the maximum entropy method (MEM) of obtaining complex SFG spectra from homodyned experiments, they also proposed that the depth information is entirely contained within the associated error phase that generally complicates such analysis, therefore leading to interesting possibilities for depth-related studies. Equally, other methods which combine multiple SFG measurements from systems with altered subphase concentrations have also been proposed as an approach to separate the CL and DL contributions from charged interfaces.[70] While these methods do indeed represent progress in the separation of these multiple depth-dependent signals, it is important to note that they are not without crucial assumptions. These include, for example, equating the Stern potential that modulates the DL contribution to either the surface or zeta potentials, or that the CL contribution is unvarying with changing subphase salt concentrations. While these may well be good approximations for very specific cases, they are not generally applicable. Nevertheless, as shown later, experimental advancements in SFG spectroscopy have now made these decompositions possible without the need for such assumptions.

Another source of interference between multiple SFG contributions is that between the vibrationally resonant and nonresonant responses. These contributions are always present and can lead to difficulties in data analysis and interpretation, even for the case where there is no extended anisotropic depth, such as the air−water interface. Unlike the resonant (R) contribution which is dominated by interactions with the vibrational part of the molecular wave function and thus the asymmetry in the Morse potential, the NR contributions are dominated by higher lying states and are therefore sensitive to the asymmetry in the polarizable electron cloud.[78] In consequence, the two contributions probe vastly different aspects of the molecular structure and can thus potentially originate from different spatial regions within the interface. Additionally, the two contributions will have different spectral line-shapes, with the former vibrationally resonant part presenting strong amplitude and phase modulations as a function of frequency (due to the resonances), but the NR contribution being largely independent of the IR frequency. In phase-resolved (heterodyned) spectra the output of multiple contributions is purely a linear-superposition. Therefore, in the case of the NR contribution, it simply adds a constant offset to the spectra, as shown in eq 16. This is demonstrated in Figure 4a for the air−water (D_2O) interface which shows the real and imaginary parts of the phase-resolved spectrum. Note that, the NR contribution can clearly be seen to predominantly result in a constant negative offset in the real part.

$$S_{\text{heterodyne}} \propto \chi^{(2)}_{\text{eff}} = \chi^{(2)}_{\text{R}} + \chi^{(2)}_{\text{NR}} \tag{16}$$

In such phase-resolved SFG measurements, the presence of the NR contributions obviously does not affect peak positions and line-shapes of the resonant responses. The situation is, however, fundamentally different for intensity (homodyned) SFG measurements, which continue to be prevalent in SFG research.[79−87] The output signal is then related to the square of the effective susceptibility, as shown in eq 17, meaning the R and NR contributions interfere and can significantly alter the observed line-shape.

$$S_{\text{homodyne}} \propto |\chi^{(2)}_{\text{eff}}|^2 = |\chi^{(2)}_{\text{R}}|^2 + |\chi^{(2)}_{\text{NR}}|^2 + 2|\chi^{(2)}_{\text{R}}\chi^{(2)*}_{\text{NR}}| \tag{17}$$

While in some cases this distortion effect may well be negligible, in many prominent cases the NR contribution is significant, leading to complete deformation of the vibrational spectrum. One example of this is clearly shown in Figure 4b which presents the intensity spectrum of the overall response

https://doi.org/10.1021/acs.jpcc.4c06650
J. Phys. Chem. C 2024, 128, 20733−20750

from the air-D_2O interface, which has become the well-known showcase spectrum of the SFG technique,[10,88−90] along with the same but having removed the NR contribution through subtraction of the air-H_2O spectrum, i.e., obtained through isotopic substitution measurements (green trace).[24,91] This comparison shows that the line-shape and peak positions of the SFG intensity spectrum are drastically affected by the interference of the R part with the NR contribution, making it in fact a poor and misleading representation of the vibrational spectrum of the interface without correction for the NR background. The resulting spectral distortions are meanwhile quite comparable to the distortions originating from the phase-shifts discussed above. As the NR contribution is predominantly located in the real part of the response, the interference makes some part of the dispersive resonant line-shape enter the intensity spectrum. If only such an overall intensity spectrum is obtained from a measurement, the interference effect can only be removed by correctly decomposing the spectrum into its R and NR contributions by performing a multiparameter fit. To obtain reliable results from such a fit, however, significant prior knowledge of the center-frequencies and spectral shapes of the different resonant features is required. For a complex system such as the air−water interface, such knowledge is generally not available. The impact of the NR contribution on the resonant line-shape has therefore often been neglected, which has e.g. resulted in the misled initial assessments of the air−water interface spectrum, where the large red-shifted peak (here at ∼2500 cm^{-1} for D_2O) was interpreted as being indicative of significant "ice-like" water that is strongly H-bonded.[88,92] More recently, the strong interference effect with the NR contribution and the resulting spectral distortions has been noted,[10,93] and this structural interpretation was shown to be inaccurate, with the main H-bonded resonance being substantially higher in frequency, more in-line with the expectation of liquid water.

From the discussion above, it is clear that the analysis of SFG spectra can become highly demanding whenever multiple contributions are present. This is particularly true for homodyned intensity SFG measurements where no phase resolution is obtained. In the case of complex sample systems including multiple depth contributions, such as charged aqueous interfaces, it is therefore evident that phase-resolved (heterodyned) SFG has substantial benefits over conventional intensity approaches.

3.3. Quadrupolar Contributions. In all of the discussion above, just as with the vast majority of SFG research, the output signals are assumed to arise from structurally anisotropic regions, i.e., from a thin region at the interface (for most media such as water). This assumption thus only considers the purely electric dipole-driven transitions (EDA) and neglects any higher order spatial contributions. Beyond this approximation, however, second-order signals can also arise from electric quadrupolar-driven transitions which, despite their generally lower transition probabilities, can become significant as they are not restricted to structurally anisotropic regions.[7,21] This means that they are not subject to the cancellation of signals from oppositely oriented molecules and can thus, in principle, yield signals from in-plane molecules and even throughout the entire bulk. Unlike the dipolar contribution which arises from the coupling of the electric fields of the two incident fields, the electric quadrupolar contributions source from the coupling between a field and a field gradient.[7,21,94] In this sense, there are two aspects of the electric fields that lead to field gradients which can yield quadrupolar signals. First, there is the sharp change in field amplitude that occurs at the interface due to the anisotropy in the dielectric function (i.e., the gradient in the local field factors). This contribution is hence tightly bound to the interface, with a depth profile of only a few angstroms, and is thus named the interfacial or anisotropic quadrupolar signal (IQ). While this signal only arises from a few molecular layers, it could become significant due to the sheer magnitude of the field gradient at the interface. Second, there is the field gradient arising from the oscillatory nature of the field, which clearly persists throughout the entire medium, yielding a bulk or isotropic quadrupolar contribution (QB). A schematic of the source mechanisms and different spatial origins of the different contributions is illustrated in Figure 5.

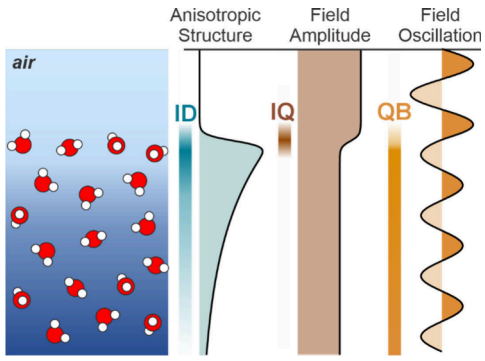

Figure 5. Schematic showing the spatial and mechanistic origins of the electric dipolar and quadrupolar signals to the overall SFG response. ID: interfacial dipole, IQ: interfacial quadrupole, QB: bulk quadrupole.[7]

The presence of either contribution interfering with the purely dipolar (structurally anisotropic) signal complicates the analysis for several reasons. First, the quadrupolar contributions are governed by rank-4 tensors (due to the field gradient direction coupling into $\chi^{(2)}$) so, as mentioned above, the signs of the output signals are independent of the molecular orientation, unlike dipolar signals. Therefore, the quadrupolar spectrum arising from the same molecular environments will generally yield a different line-shape than the dipolar spectrum. Second, as demonstrated schematically in Figure 5, the three contributions generally arise from different spatial regions, and thus likely probe different molecular structures and environments. This will hence further alter their relative line-shapes. Finally, due to their different spatial profiles and mechanistic origins, the apparent depth-related phase distortions will be different. Specifically, as the IQ contribution is tightly bound to the interface, it will experience a very minimal phase distortion due to propagation effects, with the dipolar signal likely arising from a thicker region. The QB contribution in contrast contains a 90° propagation phase-shift due to its bulk origin. The intrinsic QB response is, however, also phase-shifted by 90° due to the coupling to the oscillatory component of the field gradient which leads to an overall 180° phase shift, i.e., manifesting purely as a sign-flip in the local response.[7,24] It will therefore show similar behavior as a purely interfacial signal from electric dipolar sources, with no mixing between real and imaginary parts. This property makes it in turn very challenging to distinguish the two contributions (interfacial and bulk) and to extract the typically desired interfacial response of the system. The most characteristic difference between the dipolar and the QB responses is their different spatial origin which further underlines the necessity to obtain depth information on the SFG signal sources.

https://doi.org/10.1021/acs.jpcc.4c06650
J. Phys. Chem. C 2024, 128, 20733−20750

As many structural investigations of interfaces rely on the interpretation and comparison of experimental SFG spectra to the analogous calculations from simulations, it is also important to mention that many simulations, including those yielding the results shown in Figure 1, typically do not fully address the quadrupolar contributions. This hence limits the possible insights into the structural motifs present at the interface that can be obtained from quantitative or even qualitative comparison to calculated SFG spectra. For such comparisons, it is clearly crucial to include all potential contributions to the observed signals.

The analysis of SFG spectra in terms of quadrupolar signal contributions is further hampered by the fact that the size of the quadrupolar moments can highly vary with infrared frequency. This means different vibrational modes as well as the NR contribution may have largely different weightings between the dipolar and different quadrupolar signals. For aqueous systems, this variability across different spectral transitions seems to be substantial, with the NR contribution having been previously suggested from both experimental measurements and accompanying theory to be dominated by quadrupolar contributions, with a particularly significant role from the IQ mechanism,[95,96] and more recently being experimentally shown to have also have a significant QB contribution.[24] By contrast, the OH stretching mode of water (R contribution) seems to mainly arise from dipolar signals owing to its blue-shifted frequencies being indicative of a weaker H-bonding environment (as expected for the interface), as well as the observed sign-flip for oppositely oriented molecules. This too differs from the resonant H−O−H bending mode which, like the NR contribution, also appears to be dominated by quadrupolar signals.[97] Such observations highlight that the role of quadrupolar contributions in SFG investigations, particularly for aqueous interfaces, cannot be simply neglected, and must be treated separately for each feature of the overall response.

4. RECENT DEVELOPMENTS IN PROBING AQUEOUS INTERFACES

In the discussion above, various challenges associated with SFG measurements have been identified. A key point within this discussion is the role of signal contributions from extended sample depths as well as the necessity to acquire such depth information for a correct interpretation of SFG spectra and to obtain detailed understanding of interfacial molecular structures. Additionally, the importance of separating different signal contributions such as R and NR responses was emphasized. Recently, several advancements in SFG spectroscopy have been developed to address these challenges and we review and discuss a selection of the most promising approaches among these developments.

One very crucial technical advancement and milestone in SFG spectroscopy already dates back more than two decades, namely the advent of phase-sensitive measurements.[9,98−101] The clear advantage of this technique is twofold: first, it doubles the information content of measured SFG spectra by revealing amplitude and phase information, and second, it makes all different signal contributions become linearly superimposed in the final spectra without the rise of any complex interference terms between them. This linearity highly simplifies the data analysis and allows for performing advanced measurements protocols such as difference spectroscopy in a straightforward manner.[24,102] Like for all vibrational spectroscopy techniques, isotope labeling approaches are of particular importance in this context because this enables the unambiguous identification of molecular species and the decomposition of congested spectra into specific vibrational modes.[103,104] Furthermore, comparison between vibrational spectra of different isotopologues also allows for the precise decomposition of SFG spectra into the vibrationally resonant and nonresonant parts, as demonstrated with the example of the air−water interface in Figure 4 and in reference.[24,91] It should be noted that the additional phase information obtained in phase-sensitive measurements in principle also already contains the desired depth information which is encoded in the propagation phase. However, from such measurements alone, the propagation phase cannot be isolated as it is convoluted with the intrinsic spectral phase of the vibrational resonances.[36,37] For the determination of the propagation phase, additional information from experimental measurements or from theory is therefore required.

One powerful experimental concept to directly obtain depth information from SFG measurements is the modulation of the coherence length. While the entangled nature of the material properties with experimental parameters due to signal contributions from extended sample depths is, on the one hand, not ideal for isolating the structural properties from the interface, it does, on the other hand, provide a useful route for accessing the depth dependency of the susceptibility, and thus the depth-dependent structure. As discussed earlier, signal contributions from below the interface contain the propagation phase factor, $e^{i\Delta k_z z}$ which, after integration in z, leads to phase-shifts and amplitude changes in the observed spectrum.[36] An illustration of the evolution of spectral amplitude and propagation phase with increasing anisotropic depth is given in Figure 6a for two selected values of Δk_z. From this plot two things become apparent: first, both observables clearly vary with the anisotropic depth, as expected, and second, they also both highly depend on the value of Δk_z. Therefore, by modulating the coherence length, $1/\Delta k_z$, the depth information becomes in principle separable from the intrinsic (local) susceptibility. Obviously, for the best sensitivity of this method, the modulations should be as large as possible. The scale of the differences in these two observables are depicted in Figure 6b which shows the resulting amplitude ratio (black) and phase difference (red) as a function of anisotropic depth for the two selected values of the coherence length (see Supporting Information for more details). While these plots are clearly not generally applicable to all experimental settings and sample systems, they nonetheless give an idea of the expected modulations that would be observed for an interface with a given anisotropic depth.

Interestingly, while the amplitude scales with the modulus of the coherence length, the resulting phase-shift scales with Δk_z (inverse of coherence length), including its sign. Therefore, two different modulation regimes exist for the phase, which are each presented in Figure 6b: one with the same signs of the two Δk_z values (shown in solid red), and one with opposite signs (shown in dashed red). The three presented plots in Figure 6b thus highlight two important points. First, the phase difference and amplitude ratio show different functional forms. Therefore, the information contained in both are complementary and not degenerate. In consequence, while the depth information can clearly be extracted from either observable for the case where the response can be described simply by a single depth-related parameter, e.g. an exponential decay function, for more complex systems that involve multiple depth-dependent contributions, one observable is generally insufficient. In this context, it is

https://doi.org/10.1021/acs.jpcc.4c06650
J. Phys. Chem. C 2024, 128, 20733−20750

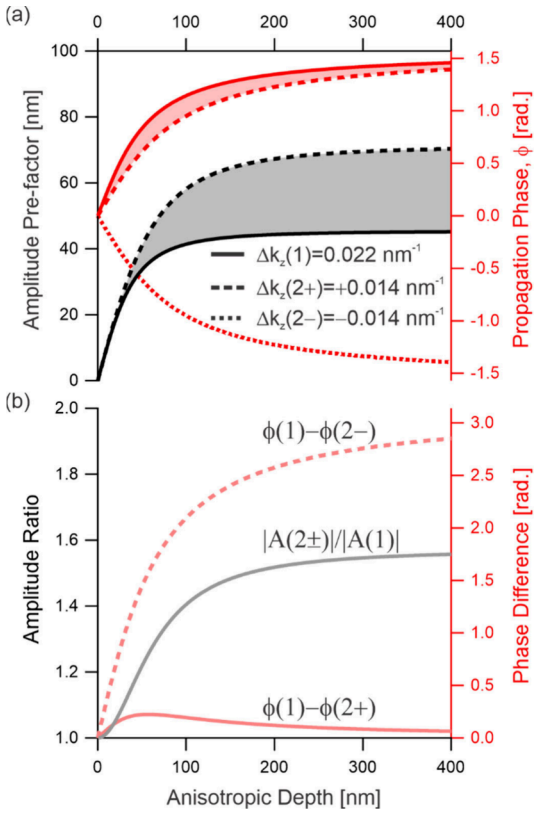

Figure 6. Amplitude and phase variations of the observed SFG signal due to depth. (a) Plots of the amplitude scaling and propagation phase shift for two different coherence lengths that are typical for SFG studies of aqueous interfaces. While the amplitude prefactor is only shown for two wavevector mismatches, as it independent of sign, the propagation phase is presented with $\Delta k_z(2)$ taking either a positive or negative value, indicated by the two labels $\Delta k_z(2+)$ and $\Delta k_z(2-)$. (b) Resulting amplitude ratios and phase differences between the observed signals with these coherence lengths, showing the different cases for equal and opposite signs for the two Δk_z values, i.e., $\phi(1) - \phi(2+)$ and $\phi(1) - \phi(2-)$, respectively, for the phase differences (with the amplitude ratio being independent of sign). Further details on these plots can be found in the Supporting Information.

important to note that most systems of interest, e.g. charged interfaces, multiple contributions are present. Therefore, combining both pieces of information allows for a more accurate characterization of the depth-dependent $\chi^{(2)}(z)$, for example, the unambiguous identification of any bulk signals with quadrupolar origin.[24] The second important point highlighted by Figure 6b is associated with the vastly contrasting phase difference plots for the equal and opposite sign wavevector mismatches. This shows that having opposite signs yields overall much higher depth sensitivity in the phase difference, gives sensitivity to both small and large depths, and importantly presents a monotonic function which yields a clear 1-to-1 relationship to the anisotropic depth. Nevertheless, while having opposite signs for Δk_z is clearly favorable, this is not generally the case for techniques exploiting the coherence length modulation, as discussed below.

4.1. Transmission/Reflection SFG. Modulation of the coherence length was first highlighted by Shen et al., who discussed the principle of measuring the SFG intensity in both reflection and transmission to determine the isotropic quadrupolar contributions that arise throughout the entire bulk.[105] As the output SFG wavevector has opposite signs for the z-components in reflection and transmission, such measurements represent a substantial modulation of the coherence length of typically 3 orders of magnitude (but Δk_z stays generally positive). This hence leads to a large amplitude modulation in the spectra for any bulk contributions, which allowed the authors to completely disentangle them from the surface SFG signal of the benzene-air interface. Clearly, this approach can be very powerful for separating interfacial and bulk contributions (e.g., dipolar vs quadrupolar) and, although it has not been demonstrated yet, also has significant potential for obtaining depth-dependent structural information from the interface. Equally, while it has only been performed using intensity measurements (i.e., only using the amplitude information), extracting the phase information would also lead to greater structural insight, as mentioned above. Recording both the reflection and transmission responses has, however, not become a widely adopted experimental approach due to its associated significant experimental challenges, particularly with obtaining accurate phase information from both signals. Additionally, the large coherence length obtained for the transmission signal leads to the necessity to account for additional effects such as pump beam depletion which makes the data analysis more complex.

4.2. Variable-Angle SFG. While the principle of modulating the coherence length for obtaining depth-dependent structural information at charged interfaces was first mentioned by Shen and Tian,[54] its was not until recently that it was experimentally demonstrated. Three alternative approaches have been presented, with each being used to study the depth-dependent structure at aqueous interfaces. Hore and co-workers showed the initial approach where the incident angle of the input beams is altered, thus modulating the specific z-component of their wavevectors.[63,106,107] This can be done in full reflection geometry and hence circumvents the challenge of detecting the transmitted beam. Furthermore, by using an internal reflection geometry that includes the critical angle, the authors showed that the coherence length can be significantly modulated, which is not the case for regular reflection geometries. This hence allows for high depth accuracy, especially as the variable-angle (VA-SFG) approach can generate many unique data points. The authors demonstrated this technique by successfully separating the CL and DL spectra from such angular-dependent intensity measurements and compared the water structure in the corresponding regions, clearly highlighting the potential of this method. The challenges associated with this technique are that it requires multiple subsequent measurements rather than simply recording multiple responses from a single experiment, and involves an elaborate sample geometry. Additionally, the internal reflection approach restricts the classes of interfaces that can be investigated, and proximity to the critical angle means the output signals become very sensitive to local field effects which must be correctly accounted for. Finally, obtaining accurate phase information with this technique would also be analytically challenging due to the strong angular-dependence on the reflection phase of any reference.

4.3. Frequency (Momentum)-Dependent SFG. As the second approach, Hsiao et al. performed momentum-dependent SFG (MD-SFG) whereby they modulated the frequency of the visible upconversion beam, and thus the magnitude of its wavevector.[29] That way, the depth information also becomes accessible, which was demonstrated by extracting the CL spectrum from the overall water response at charged interfaces using the combination of intensity and phase-resolved spectra.

https://doi.org/10.1021/acs.jpcc.4c06650
J. Phys. Chem. C 2024, 128, 20733−20750

The distinct benefit of this approach is that it does not require a complex sample setup (like the variable-angle approach), and also is not restricted to certain sample classes. Furthermore, just as the variable-angle technique, it provides the opportunity to record several unique data points to extract the depth information. In principle, this approach could also include the analysis of the phase changes due to depth to further increase the analytical capabilities, although this has not been demonstrated. Nevertheless, multiple separate measurements are again required and, as this technique involves altering the frequencies, it is subject to potential dispersion effects which can make the spectral corrections and analysis more challenging. While for relatively small changes in frequency these are minor effects, this is counter to achieving large coherence length modulations, meaning a compromise must be made. Finally, in contrast to the other methods, MD-SFG cannot effectively separate interfacial and bulk signals since the bulk quadrupolar response is highly insensitive to upconversion frequency.[24]

4.4. Combining Sum- and Difference Frequency Generation (SFG/DFG). The third approach for extracting depth information from the modulation of the coherence length is a recent development combining SFG measurements with their corresponding DFG responses.[24,36,37] For probing the same resonant vibrational information, the SFG and DFG responses not only have different magnitude wavevector mismatches, but they also differ in sign. The different magnitudes (SFG and DFG signals differ in frequency) is analogous to the momentum-dependent approach, and therefore can obtain similar insight from the amplitude modulations. Beyond this, however, the different signs of the two wavevector mismatches is a unique feature of this approach and makes the phase difference a far more sensitive parameter for depth-dependent studies (as shown above). As a result, SFG/DFG can obtain exceptional depth accuracy, with phase-resolved studies having been shown to achieve sub-nanometer resolution on model systems of self-assembled monolayers on quartz,[36] as well as being used to extract the first experimental measurement of the anisotropic "healing depth" of the air−water interface.[24] The SFG/DFG method also benefits from the fact that both responses are simultaneously generated, meaning the depth information can be extracted from a single measurement, in contrast to the two aforementioned techniques. Furthermore, as bulk quadrupolar contributions have different amplitudes in SFG and DFG pathways, the bulk signals can also be separated from the interfacial response and their mechanistic origin (dipolar/quadrupolar) identified.[24] One particular additional benefit of SFG/DFG that contrasts to the MD-SFG or VA-SFG, is that other phase distortions to the spectra arising from complex high frequency Fresnel factors can also be completely removed as they too modulate the SFG and DFG responses differently.[37] While this may not be especially relevant to many aqueous interfaces, it is crucial whenever they are in the presence of media which absorb in the visible frequencies, such as metals. This hence makes it particularly important for electrochemical systems.

An example of the effectiveness of the SFG/DFG method is shown in Figure 7 which presents both the real and imaginary parts of the heterodyned SFG and DFG spectra in the O−H stretching region for the air-H_2O interface covered with a negatively charged surfactant, dihexadecylphosphate (DHP). This is shown for two subphase salt concentrations, 0.1 M (Figure 7a) and 10^{-4} M (Figure 7b), which have substantially different Debye screening lengths, namely 1 and 30 nm,

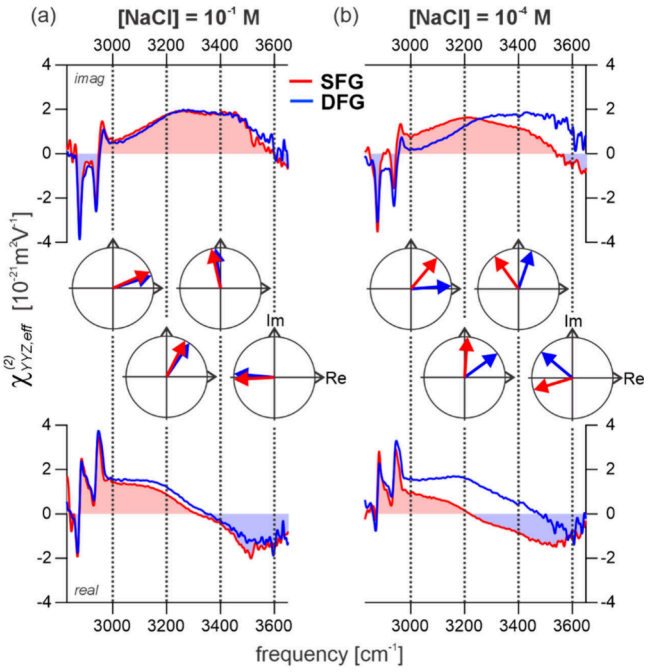

Figure 7. Heterodyned SFG and DFG spectra recorded in the SSP polarization combination from the air−water interface covered with negatively charged surfactants (DHP), showing both the real and imaginary parts for a subphase NaCl salt concentration of (a) 10^{-1} M and (b) 10^{-4} M. Also shown are schematic Argand plots of the SFG and DFG phases at selected frequencies through the resonant line shape.

respectively. Since the SFG and DFG responses probe the same susceptibility, they have the same intrinsic line-shapes, only that they are phase-shifted in opposite directions owing to the different signs of their wavevector mismatches. By representing the responses schematically in phase diagrams (Argand plots) at four different frequencies through the O−H stretching region, Figure 7 demonstrates that the phase difference between SFG and DFG is both maintained, and evidently scales with the screening length, as expected. This clearly highlights that important depth information about the interfacial region can be separated and extracted from the two spectra, including the separation of the CL and DL contributions, just as for MD-SFG and VA-SFG.

While there are clearly many benefits for SFG/DFG, it too comes with challenges. First, and perhaps the most important of which is that, in order to extract the full benefits of the technique by measuring not only the amplitudes but also the phases of the two nonlinear responses, exceptional accuracy in both the absolute phase and exact frequencies of both responses is required. This hence makes for an extraordinary experimental challenge and means the technique cannot feasibly be implemented into any standard SFG spectrometer, but instead requires a more specialized setup. Beyond this, due to the different output frequencies of SFG and DFG, it too (just like the MD-SFG) is subject to potential dispersion effects. With the given frequency differences between SFG and DFG, however, these effects are usually negligible and, if not, can be effectively removed by recording SFG and DFG with the same three frequencies in separate measurements (although this procedure loses the above-mentioned simultaneity benefit).[24,37]

4.5. Summary of Coherence Length Modulation Techniques. While the four techniques presented above follow the same principle (modulation of the coherence length/

https://doi.org/10.1021/acs.jpcc.4c06650
J. Phys. Chem. C 2024, 128, 20733−20750

wavevector mismatch), the resulting spectral modulations in phase and amplitude of the measured spectra can be distinctly different. A general evaluation of their efficacy in extracting depth information is not straightforward as the achieved modulations highly dependent on both the specific properties of the sample systems and realistic experimental limitations. To give some comparative indication of their performance, we turn to the example of charged aqueous interfaces due to their widespread relevance in such studies. In Figure 8 we compare

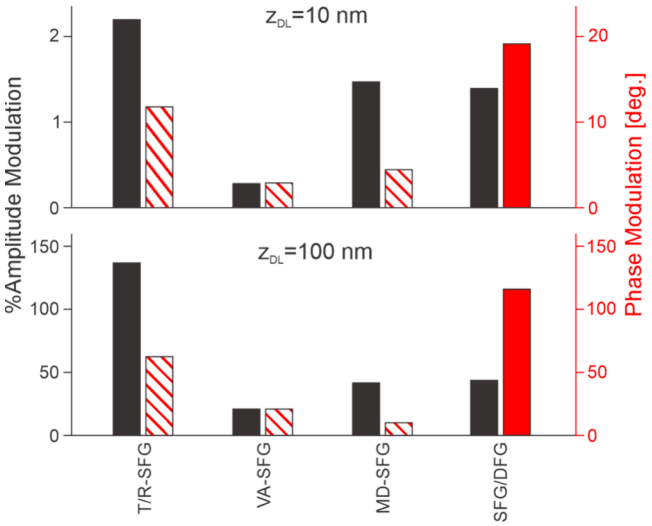

Figure 8. Comparison of the amplitude (black) and phase (red) modulations of the different methods for accessing depth information from modulating the coherence length. The values for the plots are shown for two different anisotropic depths that are typical values for charged interfaces, with Debye lengths of 10 and 100 nm which occur for electrolyte concentrations of 1 mM and 10 μM, respectively. The plots are based on calculations described in the Supporting Information using values for the coherence lengths from the literature.[24,29,63] The red striped bars indicate the potential phase differences using these literature values; however such phase-resolved measurements having not been demonstrated. T/R: transmission/reflection, VA: variable-angle, MD: momentum (frequency)-dependent.

the percentage amplitude modulations and absolute phase differences for the different techniques, using values for their wavevector mismatches taken from the literature.[24,29,63] This comparison is shown for diffuse layer contributions with two different Debye screening lengths, Z_{DL}, 10 and 100 nm. These modulations are calculated based on the differences in amplitudes and phases of the two measured responses for an interface with the specified depth i.e., the difference in amplitude and phase between the transmitted and reflected SFG responses from such an interface, or the differences between SFG for two different incidence angles, etc. (see Supporting Information for more details). The striped red boxes represent the theoretical phase differences as they have not been reported due to the lack of corresponding phase-resolved measurements for these techniques.

From the plots in Figure 8, it becomes clear that for the selected examples, two techniques particularly stand out, namely the T/R-SFG and combined SFG/DFG methods. It is important to mention again that these evaluations only refer to the selected examples. For the typically more complex systems, such analysis could lead to different weightings, so the optimum technique for a specific investigation can only be evaluated on a case-by-case basis, especially considering the unique experimental challenges and restrictions associated with each method.

4.6. Other Methods. Beside the coherence length modulation methods, there have been alternative ways presented of obtaining depth information. However, these either include various degrees of theoretical simulations and models, or only probe isolated aspects of the depth-dependent structure.

Recently Nagata et al. showcased a technique exploiting polarization-dependent measurements to distinguish between resonances which source from different dielectric environments.[108,109] Specifically, the z-dependence of the dielectric function is contained within the Fresnel corrections for the ZZZ contribution within the overall PPP polarization response. Therefore, by measuring both PPP and SSP polarization combinations, this contribution can in principle be isolated and, by comparison to a depth-dependent model of the dielectric environment at the interface, the depth origin of the signal can be extracted. Given that this method utilizes the variation in dielectric function across the interface, it is typically only sensitive to depth changes across the first nanometer. Using their method, the authors were therefore able to detect a height shift of ∼0.9 nm for formic acid monolayers upon increasing surface concentration.[108] One challenge with this method, however, is that it is clearly sensitive to the specific functional form of the dielectric profile across the interface and therefore replies on the accuracy of the theoretical predictions of this. As this polarization-dependent method accesses an entirely different range of structural properties at the interface, being sensitive to Ångström-scale depths rather than ∼1−100 nm for modulation of the coherence length, the two techniques could nevertheless be used simultaneously to provide complementary information about the depth-dependency of the susceptibility and gain far greater elucidation of interfacial structure.

Another recent and compelling development combines SFG with IR pump pulses, either in a traditional pump−probe scheme to record the time-dependent vibrational relaxation of the interface (TR-SFG), or in a two-dimensional spectroscopy scheme (2D-SFG) to assess intermode couplings and energy transfer mechanisms. While these techniques do not get the same level of direct depth elucidation as those discussed above, they do however gain access to enhanced structural insight through the coupling and relaxation mechanisms of the different structural motifs at the interface. By comparing these to known quantities from the bulk, therefore, some indication about the onset of bulk properties can be gained. For example, time-resolved IR pump−SFG probe measurements were utilized by the groups of Ye and Tahara to probe the T_1 vibrational relaxation time of the O−H stretching modes.[110,111] In doing so, Tahara et al. showed that the hydrogen-bonded water at the air−water interface showed strong similarities with bulk-like water, suggesting a fast onset of bulk-like behavior. By contrast, Ye et al. studied water at charged interfaces, where they used the dependency of the relaxation time on number of accessible intermolecular states to show that it can be used to assess the thickness of the CL for varying salt concentrations and species present at the interface. These indirect assessments of the depth dependency thus provide a useful alternative way of assessing the higher dimensionality of the interfacial water structure.

It is also worth noting that Benderskii et al. used an alternative approach to assess the onset of bulk properties at the air−water interface whereby they studied the vibrational coupling

https://doi.org/10.1021/acs.jpcc.4c06650
J. Phys. Chem. C 2024, 128, 20733−20750

mechanisms of the "free" OH stretch using isotopic dilution SFG measurements.[31] In doing so, they showed that these structural motifs that only exist very close to the interface are coupled solely to the other OH group on the same water molecules (intramolecular coupling). By then analyzing the stretching frequency of this coupled mode, they also showed that it displayed almost bulk-like properties. From this, just as Tahara et al. did using pump−probe SFG measurements,[111] they concluded that the onset of bulk-like properties is remarkably fast.

5. FUTURE DIRECTIONS

Over the past four decades, since its initial demonstration, vibrational SFG spectroscopy has proven to be an invaluable tool for studying interfacial structure. Within this time frame, there have been several important development steps which have brought forward its possibilities and improved the analysis of interfacial systems, but one key advancement which truly slingshot the capabilities of SFG was the introduction of phase-sensitive heterodyned detection. Because of its substantial improvement in structural insight and the fact that the first phase-resolved spectrometers have become commercially available, we expect that phase-resolved measurements will soon become the dominant SFG method.

Beyond this, the need of obtaining detailed depth information as well as a more thorough characterization of the different SFG signal contributions has become increasingly visible in the scientific community and will certainly continue to be a crucial topic in future studies. Therefore, with the techniques discussed above precisely addressing these questions, it is once again clear that a distinct and substantial improvement in the capabilities of SFG has been made. Using these methods now allows us to not only characterize the molecular constituents present at an interface along with their orientations and intermolecular connectivities, but also gain access to specific details about the depth-dependent structural anisotropy. Given that depth is an intrinsic and often important property of many interfaces, we highly anticipate these approaches to represent another significant milestone in the evolution of interfacial spectroscopy studies.

While all of the recent developments obtain similar information on depth, their sensitivities for individual aspects of the interfacial structure differ, and they each have their particular challenges, for example the applicability to only certain sample classes, sensitivity to theoretical models, or experimental complexity. While some of these challenges may well be overcome by additional development steps in the future, it is important to note that the greatest gain in insight likely lies with certain combinations of them, e.g. polarization-dependent measurements with coherence length modulation, or IR-pump-SFG/DFG-probe measurements.

One particular research field where the above techniques will be especially influential is the investigation of the molecular structure at aqueous interfaces. In these sample systems, nanoscale depth is often a significant and deterministic parameter of the interfacial properties, e.g., for charged interfaces where the existence of an electric double layer (EDL) creates a substantial variation in properties with depth. With these methodologies, the signals from aqueous interfaces can be better understood in terms of the decay lengths of their anisotropic signals, contributions from different electrostatic regimes (e.g., separating CL and DL spectra), and even isolating the purely interfacial signal from any isotropic quadrupolar contributions. Overall, this will allow for comprehensive tests of models such as the GCS model and potentially its development into more sophisticated forms which directly account for, and accurately describe the molecular response of the constituent water. Finally, the ability of the SFG/DFG method to isolate the purely resonant signals from the impact of both depth and added phases from the complex Fresnel factors shows significant promise for the study of electrochemical systems which have thus far proven to be exceptionally challenging.

■ ASSOCIATED CONTENT

Supporting Information

The Supporting Information is available free of charge at https://pubs.acs.org/doi/10.1021/acs.jpcc.4c06650.

Materials and methods used in this work, discussion on the approximations in the SFG response from charged interfaces, effect due to modulating the coherence length (PDF)

■ AUTHOR INFORMATION

Corresponding Authors

Alexander P. Fellows − *Fritz-Haber-Institut der Max-Planck-Gesellschaft, 14195 Berlin, Germany;* orcid.org/0000-0002-5885-8144; Phone: +49 (0)30 8413 5140; Email: fellows@fhi-berlin.mpg.de

Martin Thämer − *Fritz-Haber-Institut der Max-Planck-Gesellschaft, 14195 Berlin, Germany;* orcid.org/0000-0002-9631-9280; Phone: +49 (0)30 8413 5220; Email: thaemer@fhi-berlin.mpg.de

Authors

Álvaro Díaz Duque − *Fritz-Haber-Institut der Max-Planck-Gesellschaft, 14195 Berlin, Germany*

Vasileios Balos − *Instituto Madrileño de Estudios Avanzados en Nanociencia (IMDEA Nanociencia), 28049 Madrid, Spain;* orcid.org/0000-0001-7606-6653

Louis Lehmann − *Department of Physics, Freie Universität Berlin, 14195 Berlin, Germany*

Roland R. Netz − *Department of Physics, Freie Universität Berlin, 14195 Berlin, Germany;* orcid.org/0000-0003-0147-0162

Martin Wolf − *Fritz-Haber-Institut der Max-Planck-Gesellschaft, 14195 Berlin, Germany;* orcid.org/0000-0001-7226-9592

Complete contact information is available at: https://pubs.acs.org/10.1021/acs.jpcc.4c06650

Funding

Open access funded by Max Planck Society.

Notes

The authors declare no competing financial interest.

Biographies

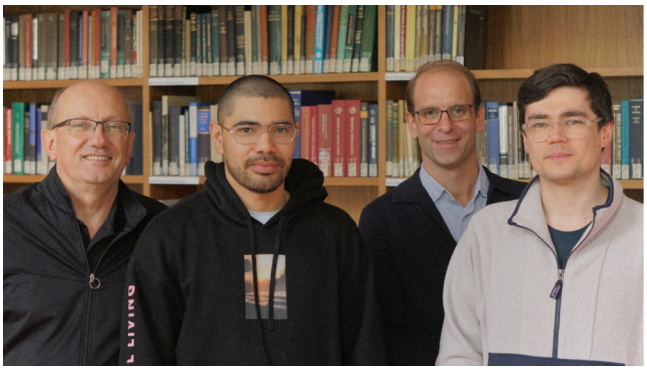

Left to right: Martin Wolf, Álvaro Díaz Duque, Martin Thämer, and Alexander Fellows.

Alexander Fellows obtained his MA and MSci in Natural Sciences from the University of Cambridge, United Kingdom, after which he stayed on to complete a PhD in Chemistry. In 2022, he commenced postdoctoral research at the Fritz Haber Institute in Berlin. His research interests surround the connection between molecular structure and macroscopic behavior at interfaces, with a particular focus on biophysical systems.

Álvaro Díaz Duque obtained his undergraduate degree in Chemistry at the National University of Colombia and his MSc. in Chemistry at the Free University of Berlin. In 2021, he started his PhD at the Fritz Haber Institute in Berlin, in the field of second-order nonlinear vibrational spectroscopy of aqueous and charged aqueous interfaces. He is interested in understanding the dynamics and thermodynamics of processes governing electrified interfaces.

Vasileios Balos received his BSc and MSc in Applied Physics from the National Technical University of Athens, Greece, after which he pursued a PhD in Physical Chemistry at the Max Planck Institute for Polymer Research in Mainz, Germany, completing it in 2017 through the University of Amsterdam. He then joined the Fritz Haber Institute in Berlin as a postdoctoral researcher for four years. In 2021, he was awarded a Marie Skłodowska-Curie Individual Fellowship, which took him to IMDEA Nanoscience in Madrid, Spain. Since 2024, he has led his own independent research group there, focusing on molecular-level liquid dynamics and processes using advanced nonlinear bulk and surface-sensitive spectroscopic techniques.

Left: Louis Lehman. Right: Roland R. Netz.

Louis Lehmann obtained a B.Sc. in Chemistry from the Technische Universität Berlin and a M.Sc. in Computational Sciences from the Freie Universität Berlin in 2021. He is currently pursuing a Ph.D. in Physics at the Freie Universität Berlin. His research focuses on the theoretical prediction of nonlinear spectroscopy in aqueous systems.

Roland Netz studied physics at the Technical University of Berlin and at MIT and received his Ph.D. in 1994 from the University of Cologne. After several postdoctoral positions he was appointed associate professor of physics at the LMU Munich in 2002 and full professor of physics at the TU Munich in 2004. Since 2011 he has held a chair in theoretical biosoft-matter physics at the Freie Universitä Berlin. His research focuses on the structure, dynamics and spectroscopy of water, proteins, polymers and charged systems using quantum, atomistic, and coarse-grained simulations as well as theoretical approaches.

Martin Wolf received his PhD at Freie Universität Berlin, Germany, with Gerhard Ertl. After a postdoc in Austin, Texas, he set up a femtosecond surface spectroscopy laboratory at the Fritz Haber Institute of the MPG and was also visiting scientist at IBM Yorktown Heights. In 2000 he was appointed as full professor in experimental physics at Freie Universität Berlin and since 2008 he is director of the Department of Physical Chemistry of the Fritz Haber Institute. His research focuses on spatial-temporal dynamics of elementary excitations at interfaces.

Martin Thämer studied Chemistry at the University of Münster, Germany and obtained his PhD in Physical Chemistry from the Technical University of Munich in 2012. After Postdoc positions at the Massachusetts Institute for Technology and the University of Chicago, he joined the Fritz-Haber-Institute in Berlin where he started a research group in 2019 that focusses on the investigation of molecular structures at interfaces using nonlinear spectroscopy and microscopy methods.

■ ACKNOWLEDGMENTS

The authors would like to acknowledge the Deutsche Forschungsgemeinschaft (DFG) for funding (Project-ID 221545957 - SFB 1078/C1).

■ REFERENCES

(1) Butt, H.-J.; Graf, K.; Kappl, M. *Physics and Chemistry of Interfaces*; Wiley-VCH Verlag: Weinheim, 2003.
(2) Ruiz-Lopez, M. F.; Francisco, J. S.; Martins-Costa, M. T. C.; Anglada, J. M. Molecular Reactions at Aqueous Interfaces. *Nat. Rev. Chem.* **2020**, *4* (9), 459−475.
(3) Benjamin, I. Molecular Structure and Dynamics at Liquid-Liquid Interfaces. *Annu. Rev. Phys. Chem.* **1997**, *48*, 407−451.
(4) Zaera, F. Probing Liquid/Solid Interfaces at the Molecular Level. *Chem. Rev.* **2012**, *112* (5), 2920−2986.

https://doi.org/10.1021/acs.jpcc.4c06650
J. Phys. Chem. C 2024, 128, 20733−20750

(5) Verdaguer, A.; Sacha, G. M.; Bluhm, H.; Salmeron, M. Molecular Structure of Water at Interfaces: Wetting at the Nanometer Scale. *Chem. Rev.* **2006**, *106* (4), 1478−1510.
(6) Shen, Y. R. *Fundamentals of Sum-Frequency Spectroscopy*; Cambridge Molecular Science; Cambridge University Press: Cambridge, 2016.
(7) Morita, A. *Theory of Sum Frequency Generation Spectroscopy*; Springer: Singapore, 2018.
(8) Boyd, R. W. *Nonlinear Optics*, 4th ed.; Pitts, T., Mearns, J., Eds.; Elsevier Inc.: London, UK, 2008; DOI: 10.1201/b18201-9.
(9) Nihonyanagi, S.; Mondal, J. A.; Yamaguchi, S.; Tahara, T. Structure and Dynamics of Interfacial Water Studied by Heterodyne-Detected Vibrational Sum-Frequency Generation. *Annu. Rev. Phys. Chem.* **2013**, *64*, 579−603.
(10) Richmond, G. L. Molecular Bonding and Interactions at Aqueous Surfaces as Probed by Vibrational Sum Frequency Spectroscopy. *Chem. Rev.* **2002**, *102* (8), 2693−2724.
(11) Yamaguchi, S.; Suzuki, Y.; Nojima, Y.; Otosu, T. Perspective on Sum Frequency Generation Spectroscopy of Ice Surfaces and Interfaces. *Chem. Phys.* **2019**, *522*, 199−210.
(12) Wang, H.-F.; Velarde, L.; Gan, W.; Fu, L. Quantitative Sum-Frequency Generation Vibrational Spectroscopy of Molecular Surfaces and Interfaces: Lineshape, Polarization, and Orientation. *Annu. Rev. Phys. Chem.* **2015**, *66* (1), 189−216.
(13) Chen, Z.; Shen, Y. R.; Somorjai, G. A. Studies of Polymer Surfaces By Sum Frequency Generation Vibrational Spectroscopy. *Annu. Rev. Phys. Chem.* **2002**, *53* (1), 437−465.
(14) Eisenthal, K. B. Liquid Interfaces Probed by Second-Harmonic and Sum-Frequency Spectroscopy. *Chem. Rev.* **1996**, *96* (4), 1343−1360.
(15) Johnson, C. M.; Baldelli, S. Vibrational Sum Frequency Spectroscopy Studies of the Influence of Solutes and Phospholipids at Vapor/Water Interfaces Relevant to Biological and Environmental Systems. *Chem. Rev.* **2014**, *114* (17), 8416−8446.
(16) Shultz, M. J.; Schnitzer, C.; Simonelli, D.; Baldelli, S. Sum Frequency Generation Spectroscopy of the Aqueous Interface: Ionic and Soluble Molecular Solutions. *Int. Rev. Phys. Chem.* **2000**, *19* (1), 123−153.
(17) Chen, Z. Investigating Buried Polymer Interfaces Using Sum Frequency Generation Vibrational Spectroscopy. *Prog. Polym. Sci.* **2010**, *35* (11), 1376−1402.
(18) Yan, E. C. Y.; Fu, L.; Wang, Z.; Liu, W. Biological Macromolecules at Interfaces Probed by Chiral Vibrational Sum Frequency Generation Spectroscopy. *Chem. Rev.* **2014**, *114* (17), 8471−8498.
(19) Hosseinpour, S.; Roeters, S. J.; Bonn, M.; Peukert, W.; Woutersen, S.; Weidner, T. Structure and Dynamics of Interfacial Peptides and Proteins from Vibrational Sum-Frequency Generation Spectroscopy. *Chem. Rev.* **2020**, *120* (7), 3420−3465.
(20) Lambert, A. G.; Davies, P. B.; Neivandt, D. J. Implementing the Theory of Sum Frequency Generation Vibrational Spectroscopy: A Tutorial Review. *Appl. Spectrosc. Rev.* **2005**, *40* (2), 103−145.
(21) Shen, Y. R. Revisiting the Basic Theory of Sum-Frequency Generation. *J. Chem. Phys.* **2020**, *153* (18), No. 180901.
(22) Patterson, J. E. The Nonresonant Sum-Frequency Generation Response: The Not-so-Silent Partner. *J. Chem. Phys.* **2024**, *161* (6), 60901.
(23) Zhang, Y.; de Aguiar, H. B.; Hynes, J. T.; Laage, D. Water Structure, Dynamics, and Sum-Frequency Generation Spectra at Electrified Graphene Interfaces. *J. Phys. Chem. Lett.* **2020**, *11* (3), 624−631.
(24) Fellows, A. P.; Duque, Á. D.; Balos, V.; Lehmann, L.; Netz, R. R.; Wolf, M.; Thämer, M. How Thick Is the Air−Water Interface?—A Direct Experimental Measurement of the Decay Length of the Interfacial Structural Anisotropy. *Langmuir* **2024**, *40* (35), 18760−18772.
(25) Morita, A.; Hynes, J. T. A Theoretical Analysis of the Sum Frequency Generation Spectrum of the Water Surface. *Chem. Phys.* **2000**, *258* (2), 371−390.
(26) Ji, N.; Ostroverkhov, V.; Tian, C. S.; Shen, Y. R. Characterization of Vibrational Resonances of Water-Vapor Interfaces by Phase-Sensitive Sum-Frequency Spectroscopy. *Phys. Rev. Lett.* **2008**, *100* (9), 96102.
(27) Nihonyanagi, S.; Ishiyama, T.; Lee, T.; Yamaguchi, S.; Bonn, M.; Morita, A.; Tahara, T. Unified Molecular View of the Air/Water Interface Based on Experimental and Theoretical $\chi(2)$ Spectra of an Isotopically Diluted Water Surface. *J. Am. Chem. Soc.* **2011**, *133* (42), 16875−16880.
(28) Inoue, K.; Ahmed, M.; Nihonyanagi, S.; Tahara, T. Reorientation-Induced Relaxation of Free OH at the Air/Water Interface Revealed by Ultrafast Heterodyne-Detected Nonlinear Spectroscopy. *Nat. Commun.* **2020**, *11* (1), 5344.
(29) Hsiao, Y.; Chou, T.-H.; Patra, A.; Wen, Y.-C. Momentum-Dependent Sum-Frequency Vibrational Spectroscopy of Bonded Interface Layer at Charged Water Interfaces. *Sci. Adv.* **2023**, *9* (15), No. eadg2823.
(30) Chiang, K.-Y.; Seki, T.; Yu, C. C.; Ohto, T.; Hunger, J.; Bonn, M.; Nagata, Y. The Dielectric Function Profile Across the Water Interface Through Surface-Specific Vibrational Spectroscopy and Simulations. *Proc. Natl. Acad. Sci. U. S. A.* **2022**, *119* (36), No. e2204156119.
(31) Stiopkin, I. V.; Weeraman, C.; Pieniazek, P. A.; Shalhout, F. Y.; Skinner, J. L.; Benderskii, A. V. Hydrogen Bonding at the Water Surface Revealed by Isotopic Dilution Spectroscopy. *Nature* **2011**, *474* (7350), 192−195.
(32) Pieniazek, P. A.; Tainter, C. J.; Skinner, J. L. Interpretation of the Water Surface Vibrational Sum-Frequency Spectrum. *J. Chem. Phys.* **2011**, *135* (4), 44701.
(33) Pezzotti, S.; Galimberti, D. R.; Gaigeot, M.-P. 2D H-Bond Network as the Topmost Skin to the Air−Water Interface. *J. Phys. Chem. Lett.* **2017**, *8* (13), 3133−3141.
(34) Mukamel, S. *Principles of Nonlinear Optical Spectroscopy*; Oxford University Press: Oxford, 1995.
(35) Wang, H. F.; Gan, W.; Lu, R.; Rao, Y.; Wu, B. H. Quantitative Spectral and Orientational Analysis in Surface Sum Frequency Generation Vibrational Spectroscopy (SFG-VS). *Int. Rev. Phys. Chem.* **2005**, *24* (2), 191−256.
(36) Balos, V.; Garling, T.; Duque, A. D.; John, B.; Wolf, M.; Thämer, M. Phase-Sensitive Vibrational Sum and Difference Frequency-Generation Spectroscopy Enabling Nanometer-Depth Profiling at Interfaces. *J. Phys. Chem. C* **2022**, *126* (26), 10818−10832.
(37) Fellows, A. P.; Balos, V.; John, B.; Díaz Duque, Á.; Wolf, M.; Thämer, M. Obtaining Extended Insight into Molecular Systems by Probing Multiple Pathways in Second-Order Nonlinear Spectroscopy. *J. Chem. Phys.* **2023**, *159* (16), No. 164201.
(38) Gonella, G.; Lütgebaucks, C.; de Beer, A. G. F.; Roke, S. Second Harmonic and Sum-Frequency Generation from Aqueous Interfaces Is Modulated by Interference. *J. Phys. Chem. C* **2016**, *120* (17), 9165−9173.
(39) Hu, X.-H.; Wei, F.; Wang, H.; Wang, H.-F. α-Quartz Crystal as Absolute Intensity and Phase Standard in Sum-Frequency Generation Vibrational Spectroscopy. *J. Phys. Chem. C* **2019**, *123* (24), 15071−15086.
(40) Thämer, M.; Garling, T.; Campen, R. K.; Wolf, M. Quantitative Determination of the Nonlinear Bulk and Surface Response from Alpha-Quartz Using Phase Sensitive SFG Spectroscopy. *J. Chem. Phys.* **2019**, *151* (6), 064707.
(41) Baldelli, S.; Schnitzer, C.; Shultz, M. J.; Campbell, D. J. Sum Frequency Generation Investigation of Water at the Surface of H2O/H2SO4 Binary Systems. *J. Phys. Chem. B* **1997**, *101* (49), 10435−10441.
(42) Medders, G. R.; Paesani, F. Dissecting the Molecular Structure of the Air/Water Interface from Quantum Simulations of the Sum-Frequency Generation Spectrum. *J. Am. Chem. Soc.* **2016**, *138* (11), 3912−3919.
(43) Wang, J.; Chen, X.; Clarke, M. L.; Chen, Z. Detection of Chiral Sum Frequency Generation Vibrational Spectra of Proteins and Peptides at Interfaces in Situ. *Proc. Natl. Acad. Sci. U. S. A.* **2005**, *102* (14), 4978−4983.

(44) Johnson, C. M.; Tyrode, E. Study of the Adsorption of Sodium Dodecyl Sulfate (SDS) at the Air/Water Interface: Targeting the Sulfate Headgroup Using Vibrational Sum Frequency Spectroscopy. *Phys. Chem. Chem. Phys.* **2005**, *7* (13), 2635−2640.
(45) Bell, G. R.; Bain, C. D.; Ward, R. N. Sum-Frequency Vibrational Spectroscopy of Soluble Surfactants at the Air/Water Interface. *J. Chem. Soc. Faraday Trans.* **1996**, *92* (4), 515−523.
(46) Ma, G.; Allen, H. C. DPPC Langmuir Monolayer at the Air-Water Interface: Probing the Tail and Head Groups by Vibrational Sum Frequency Generation Spectroscopy. *Langmuir* **2006**, *22* (12), 5341−5349.
(47) Wang, Y.; Seki, T.; Yu, X.; Yu, C.-C.; Chiang, K.-Y.; Domke, K. F.; Hunger, J.; Chen, Y.; Nagata, Y.; Bonn, M. Chemistry Governs Water Organization at a Graphene Electrode. *Nature* **2023**, *615* (7950), E1−E2.
(48) Gonella, G.; Backus, E. H. G.; Nagata, Y.; Bonthuis, D. J.; Loche, P.; Schlaich, A.; Netz, R. R.; Kühnle, A.; McCrum, I. T.; Koper.; et al. Water at Charged Interfaces. *Nat. Rev. Chem.* **2021**, *5* (7), 466−485.
(49) Geiger, F. M. Second Harmonic Generation, Sum Frequency Generation, and χ (3): Dissecting Environmental Interfaces with a Nonlinear Optical Swiss Army Knife. *Annu. Rev. Phys. Chem.* **2009**, *60* (1), 61−83.
(50) Yan, E. C. Y.; Liu, Y.; Eisenthal, K. B. New Method for Determination of Surface Potential of Microscopic Particles by Second Harmonic Generation. *J. Phys. Chem. B* **1998**, *102* (33), 6331−6336.
(51) Wang, H.-F. Sum Frequency Generation Vibrational Spectroscopy (SFG-VS) for Complex Molecular Surfaces and Interfaces: Spectral Lineshape Measurement and Analysis plus Some Controversial Issues. *Prog. Surf. Sci.* **2016**, *91* (4), 155−182.
(52) Backus, E. H. G.; Schaefer, J.; Bonn, M. Probing the Mineral−Water Interface with Nonlinear Optical Spectroscopy. *Angew. Chemie Int. Ed.* **2021**, *60* (19), 10482−10501.
(53) Covert, P. A.; Hore, D. K. Geochemical Insight from Nonlinear Optical Studies of Mineral−Water Interfaces. *Annu. Rev. Phys. Chem.* **2016**, *67*, 233−257.
(54) Wen, Y.-C.; Zha, S.; Liu, X.; Yang, S.; Guo, P.; Shi, G.; Fang, H.; Shen, Y. R.; Tian, C. Unveiling Microscopic Structures of Charged Water Interfaces by Surface-Specific Vibrational Spectroscopy. *Phys. Rev. Lett.* **2016**, *116* (1), 016101.
(55) Zhao, X.; Ong, S.; Eisenthal, K. B. Polarization of Water Molecules at a Charged Interface. Second Harmonic Studies of Charged Monolayers at the Air/Water Interface. *Chem. Phys. Lett.* **1993**, *202* (6), 513−520.
(56) Schaefer, J.; Gonella, G.; Bonn, M.; Backus, E. H. G. Surface-Specific Vibrational Spectroscopy of the Water/Silica Interface: Screening and Interference. *Phys. Chem. Chem. Phys.* **2017**, *19* (25), 16875−16880.
(57) Gouy, M. Sur La Constitution de La Charge Électrique à La Surface d'un Électrolyte. *J. Phys. Théorique Appliquée* **1910**, *9* (1), 457−468.
(58) Chapman, D. L. A Contribution to the Theory of Electrocapillarity. *London, Edinburgh Dublin Philos. Mag. J. Sci.* **1913**, *25* (148), 475−481.
(59) Stern, O. Zur Theorie Der Elektrolytischen Doppelschicht. *Zeitschrift fur Elektrochemie* **1924**, *30*, 508−516.
(60) Grahame, D. C. The Electrical Double Layer and the Theory of Electrocapillarity. *Chem. Rev.* **1947**, *41* (3), 441−501.
(61) The Electric Double Layer. In *Physics and Chemistry of Interfaces*; 2003; pp 42−56. DOI: 10.1002/3527602313.ch4.
(62) Bockris, J. O.; Devanathan, M. A. V. A. V; Müller, K. On the Structure of Charged Interfaces. *Electrochemistry* **1965**, *274* (1356), 832−863.
(63) Uddin, M. M.; Azam, M. S.; Hore, D. K. Variable-Angle Surface Spectroscopy Reveals the Water Structure in the Stern Layer at Charged Aqueous Interfaces. *J. Am. Chem. Soc.* **2024**, *146* (17), 11756−11763.
(64) Sun, S.; Schaefer, J.; Backus, E. H. G.; Bonn, M. How Surface-Specific Is 2nd-Order Non-Linear Spectroscopy? *J. Chem. Phys.* **2019**, *151* (23), 230901.
(65) Rehl, B.; Gibbs, J. M. Role of Ions on the Surface-Bound Water Structure at the Silica/Water Interface: Identifying the Spectral Signature of Stability. *J. Phys. Chem. Lett.* **2021**, *12* (11), 2854−2864.
(66) DeWalt-Kerian, E. L.; Kim, S.; Azam, M. S.; Zeng, H.; Liu, Q.; Gibbs, J. M. PH-Dependent Inversion of Hofmeister Trends in the Water Structure of the Electrical Double Layer. *J. Phys. Chem. Lett.* **2017**, *8* (13), 2855−2861.
(67) Advincula, X. R.; Backus, E. H. G.; Bonn, M.; Cox, S. J.; Diebold, U.; Fellows, A.; Finney, A. R.; Goel, G.; Hedley, J.; Jiang, Y.; et al. Electrified/Charged Aqueous Interfaces: General Discussion. *Faraday Discuss.* **2024**, *249* (0), 381−407.
(68) Ohno, P. E.; Saslow, S. A.; Wang, H.; Geiger, F. M.; Eisenthal, K. B. Phase-Referenced Nonlinear Spectroscopy of the α-Quartz/Water Interface. *Nat. Commun.* **2016**, *7* (1), 13587.
(69) Ohno, P. E.; Wang, H.; Geiger, F. M. Second-Order Spectral Lineshapes from Charged Interfaces. *Nat. Commun.* **2017**, *8* (1), 1032.
(70) Wang, Y.; Nagata, Y.; Bonn, M. Substrate Effect on Charging of Electrified Graphene/Water Interfaces. *Faraday Discuss.* **2024**, *249* (0), 303−316.
(71) Seki, T.; Yu, C. C.; Chiang, K. Y.; Tan, J.; Sun, S.; Ye, S.; Bonn, M.; Nagata, Y. Disentangling Sum-Frequency Generation Spectra of the Water Bending Mode at Charged Aqueous Interfaces. *J. Phys. Chem. B* **2021**, *125* (25), 7060−7067.
(72) Mondal, J. A.; Nihonyanagi, S.; Yamaguchi, S.; Tahara, T. Structure and Orientation of Water at Charged Lipid Monolayer/Water Interfaces Probed by Heterodyne-Detected Vibrational Sum Frequency Generation Spectroscopy. *J. Am. Chem. Soc.* **2010**, *132* (31), 10656−10657.
(73) Livingstone, R. A.; Nagata, Y.; Bonn, M.; Backus, E. H. G. Two Types of Water at the Water−Surfactant Interface Revealed by Time-Resolved Vibrational Spectroscopy. *J. Am. Chem. Soc.* **2015**, *137* (47), 14912−14919.
(74) Mondal, J. A.; Nihonyanagi, S.; Yamaguchi, S.; Tahara, T. Three Distinct Water Structures at a Zwitterionic Lipid/Water Interface Revealed by Heterodyne-Detected Vibrational Sum Frequency Generation. *J. Am. Chem. Soc.* **2012**, *134* (18), 7842−7850.
(75) Feng, R.; Guo, Y.; Lü, R.; Velarde, L.; Wang, H. Consistency in the Sum Frequency Generation Intensity and Phase Vibrational Spectra of the Air/Neat Water Interface. *J. Phys. Chem. A* **2011**, *115* (23), 6015−6027.
(76) Nihonyanagi, S.; Yamaguchi, S.; Tahara, T. Direct Evidence for Orientational Flip-Flop of Water Molecules at Charged Interfaces: A Heterodyne-Detected Vibrational Fum Frequency Generation Study. *J. Chem. Phys.* **2009**, *130* (20), No. 204704.
(77) Rehl, B.; Ma, E.; Parshotam, S.; DeWalt-Kerian, E. L.; Liu, T.; Geiger, F. M.; Gibbs, J. M. Water Structure in the Electrical Double Layer and the Contributions to the Total Interfacial Potential at Different Surface Charge Densities. *J. Am. Chem. Soc.* **2022**, *144* (36), 16338−16349.
(78) Lagutchev, A.; Hambir, S. A.; Dlott, D. D. Nonresonant Background Suppression in Broadband Vibrational Sum-Frequency Generation Spectroscopy. *J. Phys. Chem. C* **2007**, *111* (37), 13645−13647.
(79) Backus, E. H. G.; Hosseinpour, S.; Ramanan, C.; Sun, S.; Schlegel, S. J.; Zelenka, M.; Jia, X.; Gebhard, M.; Devi, A.; Wang, H. I.; et al. Ultrafast Surface-Specific Spectroscopy of Water at a Photoexcited TiO2 Model Water-Splitting Photocatalyst. *Angew. Chemie Int. Ed.* **2024**, *63* (8), No. e202312123.
(80) Wang, C.; Xing, Y.; Zhang, C.; Chen, P.; Xia, Y.; Li, J.; Gui, X. Water Structure at Coal/Water Interface: Insights from SFG Vibrational Spectroscopy and MD Simulation. *Colloids Surfaces A Physicochem. Eng. Asp.* **2024**, *688*, No. 133604.
(81) Lee, S. E.; Carr, A. J.; Kumal, R. R.; Uysal, A. Monovalent Ion−Graphene Oxide Interactions Are Controlled by Carboxylic Acid Groups: Sum Frequency Generation Spectroscopy Studies. *J. Chem. Phys.* **2024**, *160* (8), 84707.
(82) Brown, J. B.; Qian, Y.; Wang, H.; Zhang, T.; Huang-Fu, Z.-C.; Rao, Y. Quantitative Signal Analysis of Sum-Frequency Scattering

Experiments from Aerosol Surfaces. *Anal. Chem.* **2024**, *96* (33), 13607−13615.
(83) Mapile, A. N.; LeRoy, M. A.; Fabrizio, K.; Scatena, L. F.; Brozek, C. K. The Surface of Colloidal Metal−Organic Framework Nanoparticles Revealed by Vibrational Sum Frequency Scattering Spectroscopy. *ACS Nano* **2024**, *18* (20), 13406−13414.
(84) Jordan, C. J. C.; Coons, M. P.; Herbert, J. M.; Verlet, J. R. R. Spectroscopy and Dynamics of the Hydrated Electron at the Water/Air Interface. *Nat. Commun.* **2024**, *15* (1), 182.
(85) Liu, C.; Qin, X.; Yu, C.; Guo, Y.; Zhang, Z. Probing the Adsorption Configuration of Methanol at a Charged Air/Aqueous Interface Using Nonlinear Spectroscopy. *Phys. Chem. Chem. Phys.* **2024**, *26* (19), 14336−14344.
(86) Salafsky, J.; Johansson, P. K.; Abdelkader, E.; Otting, G. Ligand-Induced Conformational Changes in Protein Molecules Detected by Sum-Frequency Generation (SFG). *Biophys. J.* **2024**, *123*, 3678.
(87) Gahtori, P.; Gunwant, V.; Pandey, R. Probing the Influence of Hydrophobicity of Modified Gold Nanoparticles in Modulating the Lipid Surface Behavior Using Vibrational Sum Frequency Generation Spectroscopy. *Langmuir* **2024**, *40* (40), 21211−21221.
(88) Du, Q.; Superfine, R.; Freysz, E.; Shen, Y. R. Vibrational Spectroscopy of Water at the Vapor/Water Interface. *Phys. Rev. Lett.* **1993**, *70* (15), 2313−2316.
(89) Shen, Y. R.; Ostroverkhov, V. Sum-Frequency Vibrational Spectroscopy on Water Interfaces: Polar Orientation of Water Molecules at Interfaces. *Chem. Rev.* **2006**, *106* (4), 1140−1154.
(90) Sun, Q.; Guo, Y. Vibrational Sum Frequency Generation Spectroscopy of the Air/Water Interface. *J. Mol. Liq.* **2016**, *213* (1−3), 28−32.
(91) Ahmed, M.; Nihonyanagi, S.; Kundu, A.; Yamaguchi, S.; Tahara, T. Resolving the Controversy over Dipole versus Quadrupole Mechanism of Bend Vibration of Water in Vibrational Sum Frequency Generation Spectra. *J. Phys. Chem. Lett.* **2020**, *11* (21), 9123−9130.
(92) Du, Q.; Freysz, E.; Shen, Y. R. Surface Vibrational Spectroscopic Studies of Hydrogen Bonding and Hydrophobicity. *Science* **1994**, *264* (5160), 826−828.
(93) Raymond, E. A.; Tarbuck, T. L.; Richmond, G. L. Isotopic Dilution Studies of the Vapor/Water Interface as Investigated by Vibrational Sum-Frequency Spectroscopy. *J. Phys. Chem. B* **2002**, *106* (11), 2817−2820.
(94) Shiratori, K.; Morita, A. Theory of Quadrupole Contributions from Interface and Bulk in Second-Order Optical Processes. *Bull. Chem. Soc. Jpn.* **2012**, *85* (10), 1061−1076.
(95) Yamaguchi, S.; Shiratori, K.; Morita, A.; Tahara, T. Electric Quadrupole Contribution to the Nonresonant Background of Sum Frequency Generation at Air/Liquid Interfaces. *J. Chem. Phys.* **2011**, *134* (18), No. 184705.
(96) Shiratori, K.; Yamaguchi, S.; Tahara, T.; Morita, A. Computational Analysis of the Quadrupole Contribution in the Second-Harmonic Generation Spectroscopy for the Water/Vapor Interface. *J. Chem. Phys.* **2013**, *138* (6), 64704.
(97) Moll, C. J.; Versluis, J.; Bakker, H. J. Direct Evidence for a Surface and Bulk Specific Response in the Sum-Frequency Generation Spectrum of the Water Bend Vibration. *Phys. Rev. Lett.* **2021**, *127* (11), No. 116001.
(98) Superfine, R.; Huang, J. Y.; Shen, Y. R. Phase Measurement for Surface Infrared−Visible Sum-Frequency Generation. *Opt. Lett.* **1990**, *15* (22), 1276−1278.
(99) Superfine, R.; Huang, J. Y.; Shen, Y. R. Experimental Determination of the Sign of Molecular Dipole Moment Derivatives: An Infrared—Visible Sum Frequency Generation Absolute Phase Measurement Study. *Chem. Phys. Lett.* **1990**, *172* (3), 303−306.
(100) Shen, Y. R. Phase-Sensitive Sum-Frequency Spectroscopy. *Annu. Rev. Phys. Chem.* **2013**, *64* (1), 129−150.
(101) Yamaguchi, S.; Otosu, T. Progress in Phase-Sensitive Sum Frequency Generation Spectroscopy. *Phys. Chem. Chem. Phys.* **2021**, *23* (34), 18253−18267.
(102) Xu, X.; Shen, Y. R.; Tian, C. Phase-Sensitive Sum Frequency Vibrational Spectroscopic Study of Air/Water Interfaces: H2O, D2O, and Diluted Isotopic Mixtures. *J. Chem. Phys.* **2019**, *150* (14), No. 144701.
(103) Sathyanarayana, D. N. *Vibrational Spectroscopy: Theory and Applications*; New Age International (P) Ltd.: New Delhi, 2004.
(104) Lagunov, O.; Drenchev, N.; Chakarova, K.; Panayotov, D.; Hadjiivanov, K. Isotopic Labelling in Vibrational Spectroscopy: A Technique to Decipher the Structure of Surface Species. *Top. Catal.* **2017**, *60* (19), 1486−1495.
(105) Sun, S.; Tian, C.; Shen, Y. R. Surface Sum-Frequency Vibrational Spectroscopy of Nonpolar Media. *Proc. Natl. Acad. Sci. U. S. A.* **2015**, *112* (19), 5883−5887.
(106) Hore, D. K.; Tyrode, E. Probing Charged Aqueous Interfaces Near Critical Angles: Effect of Varying Coherence Length. *J. Phys. Chem. C* **2019**, *123* (27), 16911−16920.
(107) Cai, C.; Azam, M. S.; Hore, D. K. Determining the Surface Potential of Charged Aqueous Interfaces Using Nonlinear Optical Methods. *J. Phys. Chem. C* **2021**, *125* (45), 25307−25315.
(108) Yu, C.-C.; Seki, T.; Wang, Y.; Bonn, M.; Nagata, Y. Polarization-Dependent Sum-Frequency Generation Spectroscopy for \AA{}-ngstrom-Scale Depth Profiling of Molecules at Interfaces. *Phys. Rev. Lett.* **2022**, *128* (22), No. 226001.
(109) Yu, C.-C.; Seki, T.; Chiang, K.-Y.; Tang, F.; Sun, S.; Bonn, M.; Nagata, Y. Polarization-Dependent Heterodyne-Detected Sum-Frequency Generation Spectroscopy as a Tool to Explore Surface Molecular Orientation and Ångström-Scale Depth Profiling. *J. Phys. Chem. B* **2022**, *126* (33), 6113−6124.
(110) Tan, J.; Wang, M.; Zhang, J.; Ye, S. Determination of the Thickness of Interfacial Water by Time-Resolved Sum-Frequency Generation Vibrational Spectroscopy. *Langmuir* **2023**, *39* (50), 18573−18580.
(111) Sung, W.; Inoue, K.; Nihonyanagi, S.; Tahara, T. Unified Picture of Vibrational Relaxation of OH Stretch at the Air/Water Interface. *Nat. Commun.* **2024**, *15* (1), 1258.

https://doi.org/10.1021/acs.jpcc.4c06650
J. Phys. Chem. C 2024, 128, 20733−20750